KVN Status Report 2026

Korean VLBI Network,
Korea Astronomy and Space Science Institute

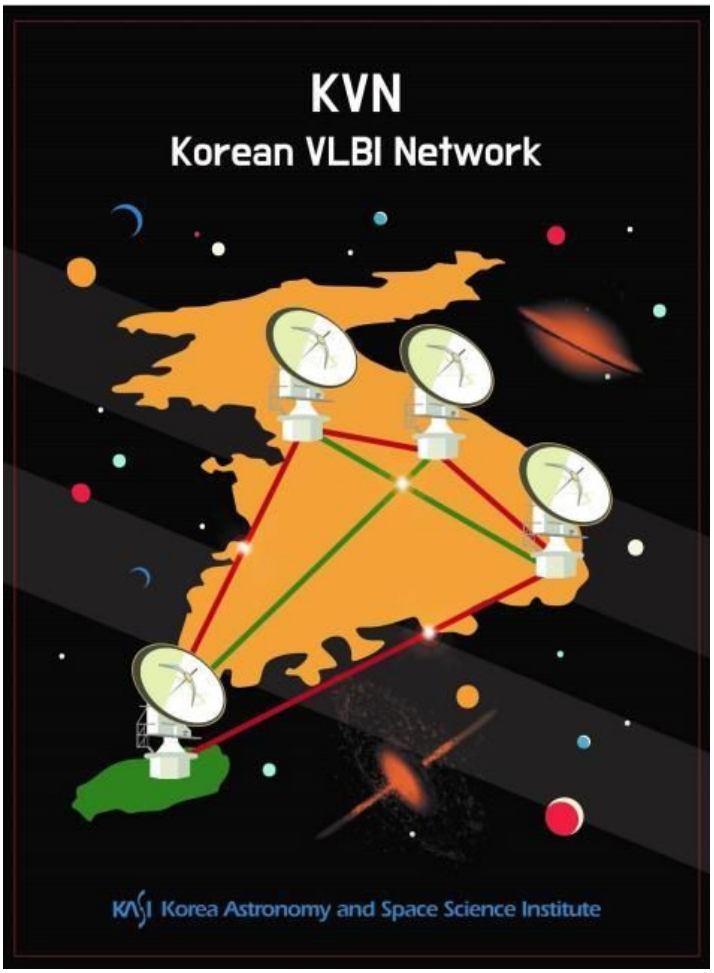

May 20, 2026
Center for KVN

Contents

List of Tables

List of Figures

1 Introduction

The Korean VLBI Network (KVN) is a Very Long Baseline Interferometry (VLBI) facility in Korea that operates at millimeter wavelengths. It consists of four 21-m radio telescopes located in Seoul, Ulsan, Jeju, and Pyeongchang, respectively: each is the KVN Yonsei Radio Telescope (hereafter KYS), the KVN Ulsan Radio Telescope (hereafter KUS), the KVN Tamna Radio Telescope (hereafter KTN), and the KVN Pyeongchang Radio Telescope (hereafter KPC). This network offers a comparable spatial resolution to a radio telescope spanning about 500 km (see Figure 1). However, it is considered a relatively modest network when compared to the larger American and European VLBI networks, such as the Very Long Baseline Array (VLBA) and the European VLBI Network (EVN). To address this limitation, KVN has developed innovative multi-frequency band receiver systems that simultaneously observe four different frequencies: K, Q, W, and D bands (with center frequencies of 22, 43, 86, and 129 GHz). In August 2013, a C band (6 GHz) receiver was installed on the KUS, which was operating in VLBI mode with the East Asia VLBI Network (EAVN) telescopes. The installation of GPS receivers at each KVN station has significantly improved the precision of phase referencing and astrometric observations. This enhancement is due to the ability of the GPS receivers to estimate atmospheric wet delays and total electron content, both of which are critical parameters for the KVN stations. Moreover, the newly built KPC has expanded its observational capabilities to cover the 230 GHz band. Since May 2025, the KPC has also been enhanced with CX, and Ka band (6 – 9 and 28 – 34 GHz) receivers in order to maximize its efficiency and performance.

This remarkable capability enables the KVN to study the formation and evolutionary processes of stars, the structure and dynamics of our galaxy, the nature of active galactic nuclei, and more, with milli-arcsecond resolution [1]. By employing such advanced technology, we have demonstrated its commitment to pushing the boundaries of scientific research and fostering collaboration among experts in the field.

- **Highlights for the 2026B call**
  - Installation of the Compact Triple-band Receiver (CTR) in the KYS was completed. The KVN has officially operated with four stations since May 2026.
  - The highest frequency bands are W-high (up to 116 GHz) in KYS and KPC, and D (up to 142 GHz) in KUS and KTN. In 2026B, only a single baseline for D band can be provided. Installation of the 150/230 GHz receiver is scheduled for the second half of 2026 in KPC and the first half of 2027 in KYS.
  - The DAS (Data Acquisition System) and the Fila10G (Fibre Link to 10 GbE) will be retired from all KVN stations during the 2026 summer maintenance. Instead, two GSM (GPU Spectrometer) and two OCTAD (OCTAve A/D Converter) will take over the roles of the DAS and the Fila10G, respectively.
    * For VLBI observations, a flexible number of IFs (up to 16×2) and the corresponding IF bandwidths (within the total recording rate) can be set for 4 frequency bands $\times$ 2 polarizations. Previously, the Fila10G forced users to set 1, 2 or 4 IFs, each with a bandwidth of 512 MHz.

* For single-dish observations, the GSM will support a much broader bandwidth mode (up to 8 GHz in total), with up to 16 IFs and 8k channels per IF. However, as the polarization stability of the GSM has not been guaranteed, it is provided on a shared-risk basis.

– The storage capacity at all KVN sites has increased from 1.25 PB to 1.75 PB by equipping two Mark6 and two Flexbuff recorders (previously two Mark6 and one Flexbuff).

– In essence, the majority of the KVN-only data will be correlated in the Halcyon correlator (GPU-based), whereas the majority of the KVN-plus-external-station data will be correlated in the DiFX correlator (CPU-based).

Figure 1: The location of the Korean VLBI Network (KVN).

2 KVN System

2.1 Network

2.1.1 Array

The KVN is a four-component VLBI network in South Korea dedicated to millimeter-wavelength VLBI observations. Four 21-m radio telescopes are strategically positioned in Seoul, Ulsan, Jeju, and Pyeongchang. The baseline lengths of these telescopes span from 133 to 506 km. All these antennas share an identical design, ensuring uniformity in their capabilities and performance (see Figure 2).

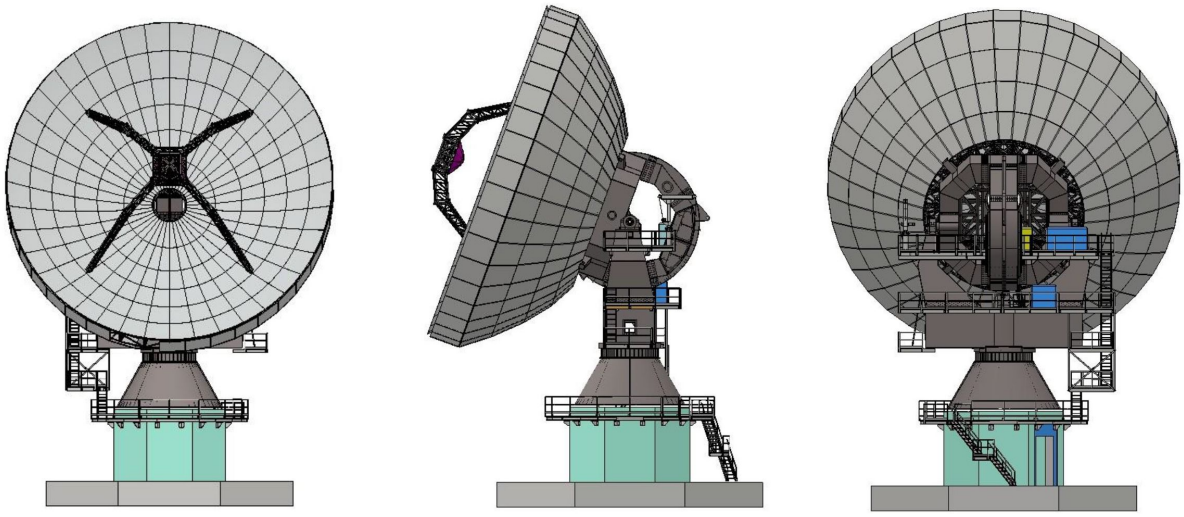

Figure 2: Design of the KVN antenna.

2.1.2 UV coverage

Figure 3 presents the simulated UV coverage of the KVN at K band for sources with varying declination (+60°, +30°, 0°, and −30°) observed over 12 hours.

2.1.3 Antenna location

Table 1 presents the coordinates of KVN antennas, while Table 2 shows the geometric locations of the four KVN stations. The position of all antennas has been determined using GPS, and KVN antenna positions are routinely monitored by GPS and geodetic VLBI observations in collaboration with VLBI Exploration of Radio Astrometry (VERA) of Japan.

2.1.4 Array Operation Center (AOC)

KVN antennas can be remotely controlled by the Array Operation Center (AOC) at the East Asia VLBI Center, KASI, Daejeon. KVN stations are interconnected with the AOC by a high-speed dedicated network called KREONET (Korea Research Environment Open

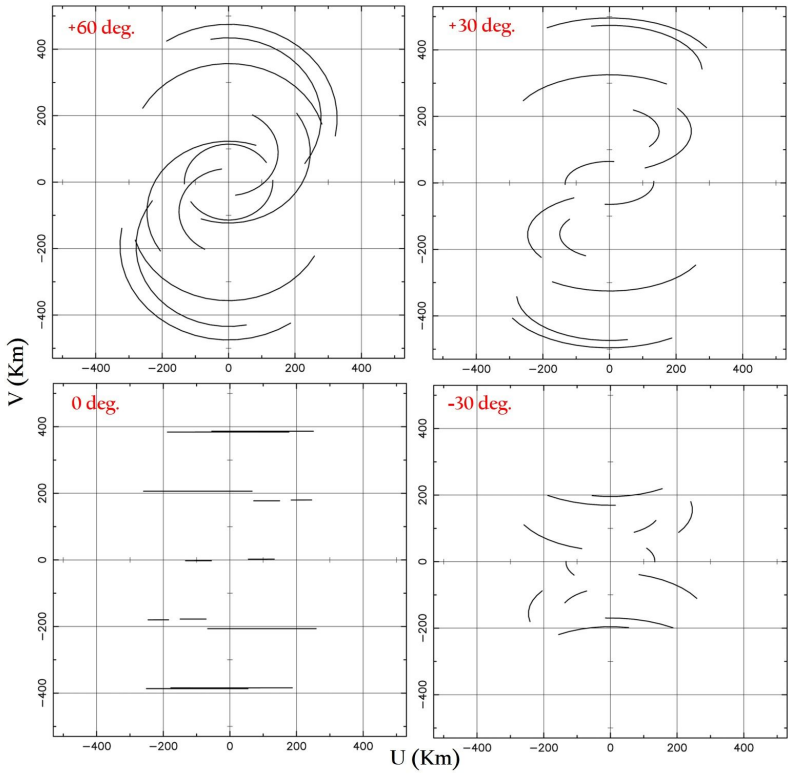

Figure 3: UV coverage simulation for the K band.

Table 1: The geographical locations of the KVN antennas

Antenna	Longitude (° ′ ″)	Latitude (° ′ ″)	Altitude (m)
KYS	126:56:27.4	37:33:54.9	139
KUS	129:14:59.3	35:32:44.2	170
KTN	126:27:34.4	33:17:20.9	452
KPC	128:26:55.1	37:32:00.1	557

Table 2: [a]Positions of KVN antennas by IVP measurement using GNSS

Antenna	Epoch	X (m)	Y (m)	Z (m)
KYS	May 08, 2024	−3042281.1397	4045902.5831	3867374.2657
KUS	May 08, 2024	−3287268.7693	4023450.0547	3687379.9226
KTN	Feb. 23, 2023	−3171731.7786	4292678.4406	3481038.7157
KPC	Dec. 14, 2024	−3149228.7899	3966414.5792	3864840.1823

[a] *The positional solution was developed on December 24, 2024, utilizing over 2,500 IVS R1R4 sessions and more than 10 EAVN sessions.*

NETwork). Considering the KVN antennas can be controlled remotely from the AOC, it is vital that the AOC operator is aware of the weather conditions that can influence the

quality of the VLBI data. Each KVN antenna has its own weather station that transmits information on air temperature, dew point, wind speed, wind direction, and air pressure to the AOC.

2.2 Antennas

2.2.1 Optics and Driving performance

The KVN antennas are shaped Cassegrain-type antennas featuring altitude-azimuth mounts. The main reflector has a diameter of 21-m and a focal length of 6.78-m. Comprising 200 aluminum panels, the main reflector achieves a manufacturing surface accuracy of approximately 65 μm. The main reflector can move at a speed of 3°/second, facilitating fast position-switching observations. The position, tilt and tip of the sub-reflector are remotely controlled and modeled to account for the effects of gravitational deformation on the main reflector and sagging of the sub-reflector. Furthermore, the newly constructed KPC antennas perform slightly better than the old KVN antennas. For further details on the antenna optics, kindly refer to Table 3.

Table 3: Specification of KVN antennas

Main reflector (Axisymmetric Paraboloid)	Parameters
Diameter	D = 21.03 m
Focal length	f $\approx$ 6.78 m
Focal ratio	f/D = 0.32
Panels manufacturing accuracy	65 μm (KVN), $\leq$ 60 μm (KPC)
Alignment surface accuracy	54 μm (KVN), $\leq$ 50 μm (KPC)
Sub-reflector (Hyperboloid)	**Parameters**
Diameter	d $\approx$ 2.25 m
Manufacturing surface accuracy	50 μm (KVN), $\leq$ 30 μm (KPC)
Expected total surface accuracy	124 μm at EL 48°
Panel	73 μm
Alignment	60 μm
Subreflector	52 μm
Backup structure	62 μm
Slewing speed	3 °/sec
Slewing acceleration	3 °/sec^2
Operating range	Az.: $-90° \sim +450°$, El.: $0° \sim 90°$

2.2.2 Gain Curve

The main reflector panels of KVN antennas were installed to give the maximum gain at the elevation angle of $\sim$ 48°. The sagging of the sub-reflector and the deformation of the main reflector by gravity with elevation results in degradation of antenna aperture efficiency

with elevation. To compensate for this effect, a hexapod is utilized to adjust the sub-reflector position in KVN antennas. Although the hexapod correction reduces significantly the dependence of aperture efficiency with elevation, the degradation still appears evidently at a higher frequency. By tracking strong maser sources or planets such as Jupiter or Mars at different altitudes, we can measure how the efficiency of the antenna changes relative to elevation. Gain curve measurements for the KPC were conducted in early 2025, while those for the KUS and KTN were conducted in January and February of this year, 2026. Meanwhile, the KYS has been upgraded to a new CTR (Compact Triple-band Receiver), similar to the KPC receiver model, and gain curve measurements were performed in April of this year.

Figure 4 shows the elevation dependency of antenna gain of all four radio telescopes measured by observing several strong maser sources and planets, utilizing the observation mode of "Five pointing" and "Cross Scan". The W-low and W-high bands measured for both of KPC and KYS correspond to frequencies of 86 GHz and 112 GHz, respectively.

We derived a normalized gain curve which has the following form: $G\_norm = A0 \cdot EL^2 + A1 \cdot EL + A2$, where EL is the elevation in degree, by fitting a second-order polynomial to the data and normalizing the fitted function with its maximum value. The fitted parameters are summarized in Table 4. The values displayed in Table 4 represent the average of Left Circular Polarization (LCP) and Right Circular Polarization (RCP).

Table 4: Coefficients of normalized gain curves (the average of LCP and RCP)

Station	Band	A0	A1	A2	Measured date
KYS	K	−5.5586E−05	3.8958E−03	9.3173E−01	2026-04-23
	Q	−3.1112E−05	2.6324E−03	9.4413E−01	2026-04-23
	W-low	−8.5063E−05	8.8374E−03	7.7138E−01	2026-04-23
	W-high	−1.9936E−04	1.7272E−02	6.2592E−01	2026-04-23
KUS	K	−1.7000E−05	1.4150E−03	9.6975E−01	2026-01-27
	Q	−1.4876E−05	1.1629E−03	9.7726E−01	2026-01-27
	W	−7.7818E−05	6.5007E−03	8.6420E−01	2026-01-29
	D	−1.5574E−04	1.4011E−02	6.8706E−01	2026-01-29
KTN	K	−1.4780E−05	1.7446E−03	9.4836E−01	2026-02-05
	Q	−1.0002E−05	1.1629E−03	9.6619E−01	2026-02-05
	W-low	−5.7710E−05	6.1485E−03	8.3212E−01	2026-02-06
	D	−1.2401E−04	1.2807E−02	6.6935E−01	2026-02-06
KPC	K	−6.0758E−06	3.2594E−04	9.9568E−01	2025-02-14
	Q	−2.5878E−05	2.5952E−03	9.3493E−01	2025-02-14
	W-low	−7.7221E−05	7.9288E−03	7.9452E−01	2025-02-14
	W-high	−1.0597E−04	1.0447E−02	7.4254E−01	2025-02-14

2.2.3 Antenna beam size and Aperture efficiency

Recently, main reflector panel alignments (using photogrammetry) were carried out fo all KVN antennas. In March 2024, an additional panel alignment was performed on the

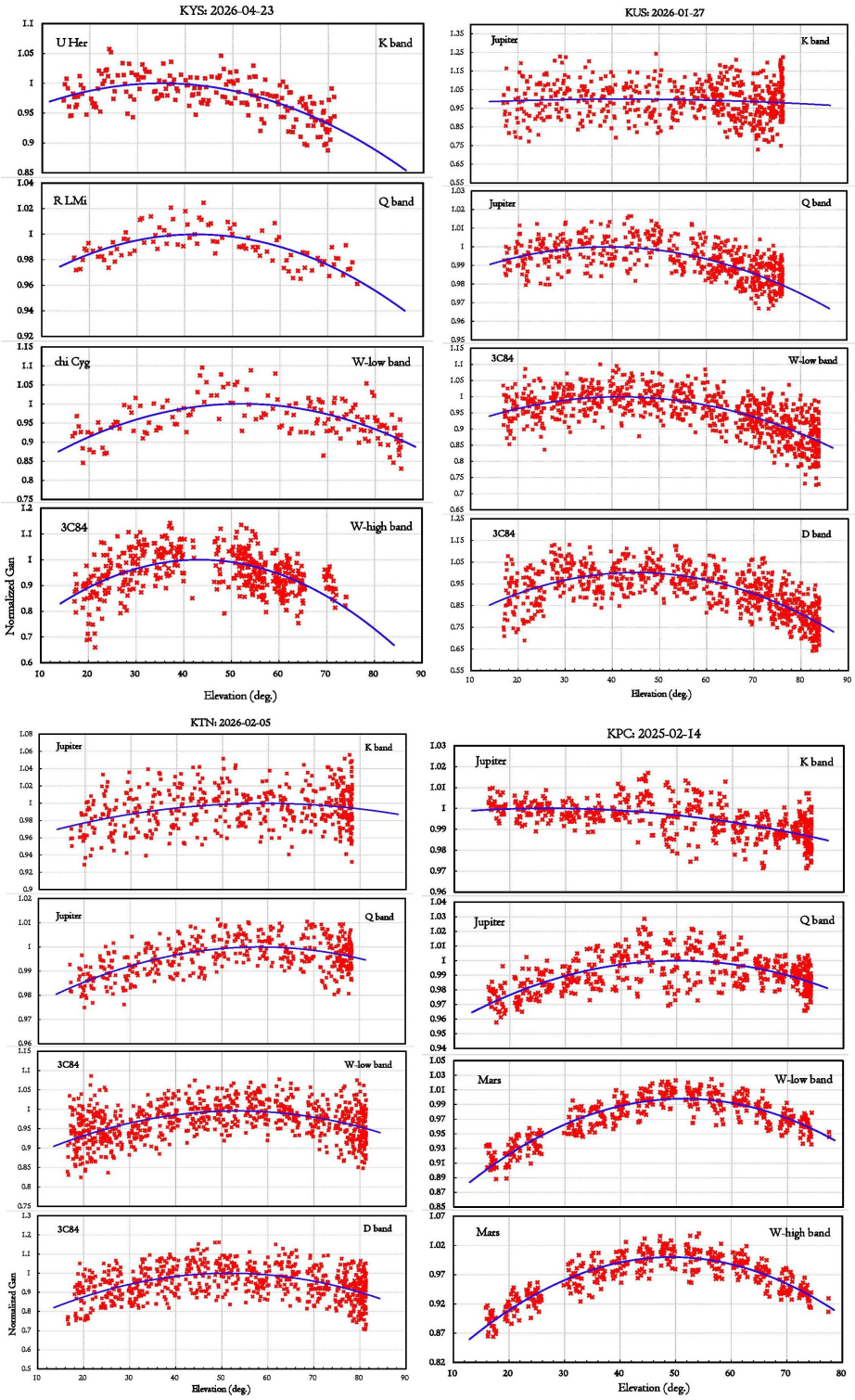

Figure 4: Gain curves of K (22), Q (43), W-low (86), W-high (110), and D (129 GHz) bands at each KVN antenna. The W-low and W-high bands in KPC and KYS correspond to 86 GHz and 112 GHz, respectively.

KYS antenna, and the sub-reflector was replaced. Furthermore, the measurement of the primary mirror panels for the recently constructed KPC antenna was completed in March 2026. Accordingly, the surface accuracies of four KVN telescopes were enhanced to 52 (KYS), 72 (KUS), 70 (KTN), and 50 (KPC) μm, respectively. Furthermore, the KVN system was recently upgraded to a wide-band receiving system employing a new sampler, the OCTAD, encompassing the frequency ranges of 18–26 GHz (K), 35–50 GHz (Q), 85–116 GHz (W), and 125–142 GHz (D), respectively (see Section 2.3). Therefore, in all wide K, Q, W, and D bands, we measured HPBW, aperture efficiency, and main-beam efficiency using the OCTAD. In the case of KYS, a significant upgrade was completed in April of this year, involving the replacement of all receivers with CTR. As a result, OCTAD-based wide band efficiency measurements have not yet been conducted.

Table 5 presents the measured results as representative values for each band. While the W and D band values were acquired through observations toward Mars and Uranus, the K and Q band values were obtained through observations toward Jupiter. The brightness temperatures for Jupiter in the K and Q bands are applied from de Pater et al. (2019)[2] and Maris et al. (2021)[3]. The estimates for the W and D bands use the Mars brightness modeling data that are displayed on its website[1]. Figure 5 displays the efficiency and beam size for each band of the telescopes.

- **Elevation dependency**
  With elevation, aperture efficiency changes. The previous section provided the gain curve that depicts the elevation dependency of the KVN antennas. The maximum values are those listed in Column (4).

- **Frequency dependency of beam efficiency**
  Beam efficiency also varies with beam size. The measured HPBWs are tabulated in Column (3), which are almost the same as the theoretical one (= λ/D of the antenna). To get a beam efficiency at 90 GHz, you have to multiply $(86/90)^2$ to that at 86 GHz.

- **Quantization correction of single-dish spectrum data**
  Prior to performing efficiency adaptations, single-dish spectrum data must be multiplied by a factor of 1.25 if it is being reduced. This is to compensate for the effects of the digital filter and spectrometer.

- Parameters of Table 5 can be applied for the following observing season;
  - KYS: from April 2026 – now
  - KUS: from January 2026 – now
  - KTN: from February 2026 – now
  - KPC: from May 2025 – now

[1] https://lesia.obspm.fr/perso/emmanuel-lellouch/mars/

Table 5: Beam size, efficiencies, and DPFU[a] of each KVN antenna

Site	Frequency (Band) (GHz)	HPBW (arcsec)	η_A (%)	η_B (%)	DPFU (K/Jy)
(1)	(2)	(3)	(4)	(5)	(6)
KYS	22 (K)	128	74	62	0.0934
	43 (Q)	65	78	63	0.0979
	86 (W-low)	33	63	51	0.0787
	111 (W-high)	27	39	39	0.0485
KUS	22 (K)	127	72	58	0.0908
	42 (Q-low)	68	73	71	0.1043
	43 (Q-high)	64	68	54	0.0856
	47 (Q-high)	61	66	57	0.0833
	86 (W-low)	32	63	47	0.0786
	95 (W-low)	29	58	45	0.0723
	111 (W-high)	26	57	45	0.0685
	115 (W-high)	26	44	41	0.0547
	129 (D)	23	53	47	0.0667
	140 (D)	21	42	38	0.0521
KTN	22 (K)	127	74	61	0.0926
	42 (Q-low)	67	70	56	0.0881
	43 (Q-high)	62	69	48	0.0866
	47 (Q-high)	58	64	48	0.0804
	86 (W-low)	32	64	48	0.0797
	95 (W-low)	28	54	38	0.0674
	111 (W-high)	26	52	44	0.0652
	115 (W-high)	24	42	32	0.0528
	129 (D)	23	54	47	0.0674
	140 (D)	21	34	29	0.0428
KPC	22 (K)	131	77	65	0.0960
	42 (Q-low)	70	78	67	0.0977
	43 (Q-high)	66	78	65	0.0981
	47 (Q-high)	60	73	60	0.0920
	86 (W-low)	34	71	62	0.0885
	95 (W-low)	33	60	59	0.0748
	111 (W-high)	25	59	48	0.0738
	115 (W-high)	26	51	46	0.0641

[a] indicates the Degree Per Flux density Unit.

η_A: Aperture efficiency, η_B: Main-beam efficiency.

2.2.4 Beam pattern

The KVN antenna optics are of the shaped-Cassegrain type, with a main reflector and sub-reflector designed to provide uniform illumination on an aperture plane. This design allows for greater aperture efficiency compared to conventional Cassegrain-type antennas.

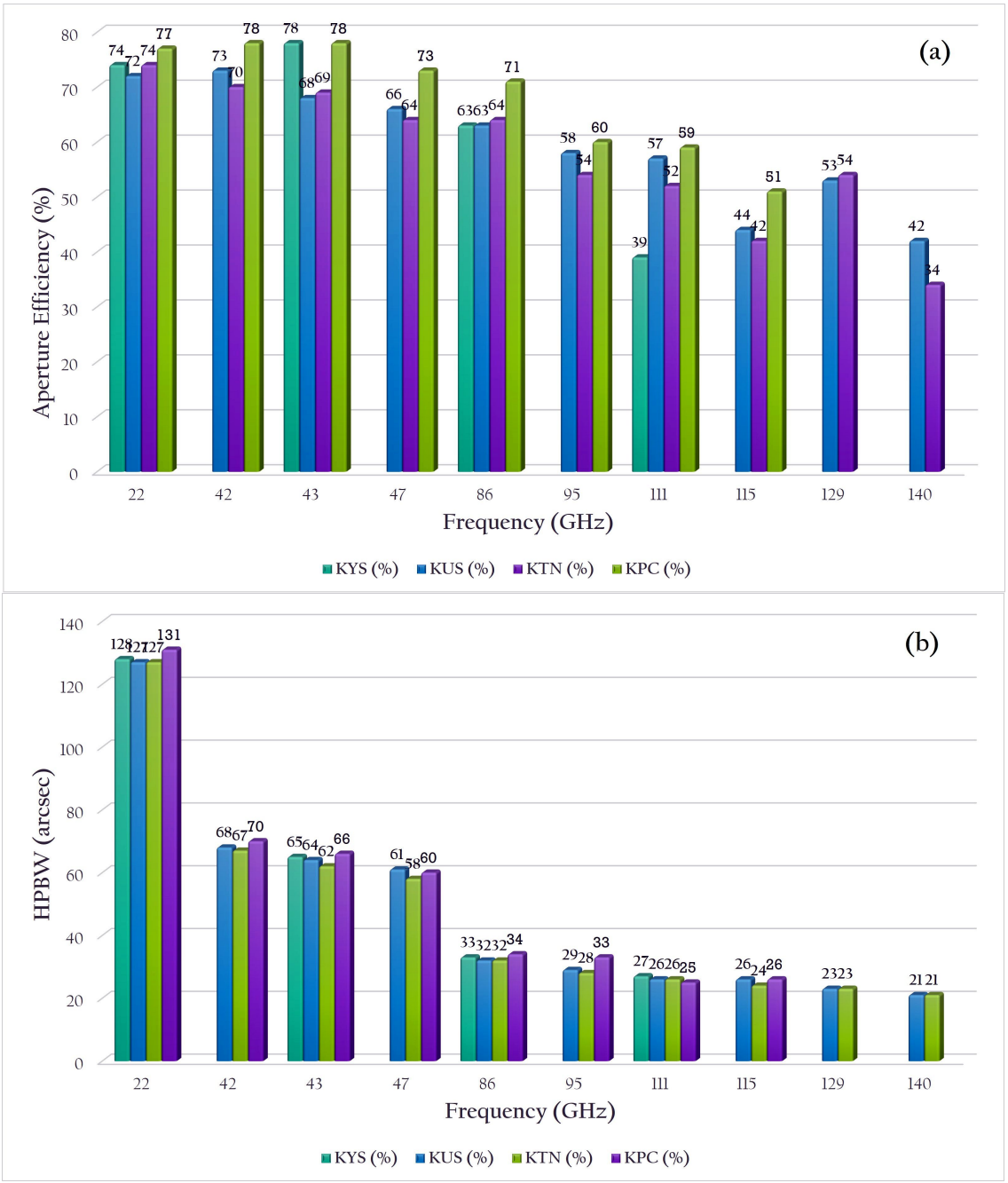

Figure 5: Aperture efficiencies and HPBWs of four KVN telescopes. (a): Aperture efficiency, (b) HPBW.

However, it should be noted that it also results in a higher sidelobe level, which may need to be taken into consideration. Figure 6 displays On-The-Fly (OTF) images of Venus and Jupiter at 86 GHz and 129 GHz, and 22 GHz and 43 GHz, respectively, as measured using the KYS antenna. The map size is $12' \times 10'$ for 22 and 43 GHz, and $3.5' \times 3'$ for 86 and 129 GHz. The first sidelobe pattern is visible. It is worth noting that KVN antennas typically exhibit sidelobe levels of -14 to -13 dB.

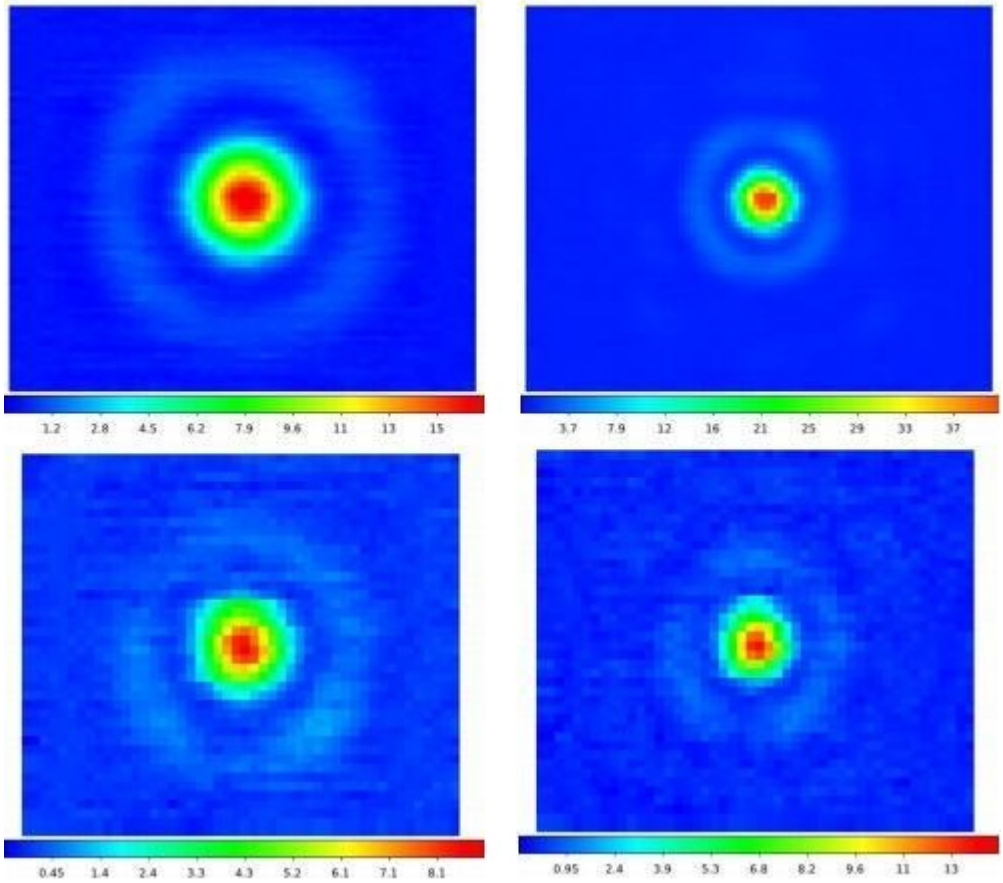

Figure 6: Beam patterns at the KYS antenna. Top panels: Jupiter at 22 GHz (left) and 43 GHz (right), Bottom panels: Venus at 86 GHz (left) and 129 GHz (right).

2.2.5 Antenna pointing accuracy

There can be systematic differences between the direction a radio telescope is intended to point and the direction it actually points. These differences can be caused by factors such as errors resulting from the telescope axis not being aligned with the true altitude-azimuth axis, deviations due to warped bearing planes, deviations due to gravitational deformation, and deviations due to non-ideal telescope construction. These systematic and recurring orientation errors are often expressed as a function of altitude and azimuth. The pointing model offers values for these errors based on altitude and azimuth to make necessary adjustments.

The KVN antenna aims for an accuracy of 4 arcseconds. In order to achieve and sustain this level of precision, periodic observations are taken to construct a pointing model. The equations of the pointing model for the KVN are given below:

$$\begin{aligned}\Delta\mathrm{A} &= \mathrm{IA} + \mathrm{CA}\ \sec(\mathrm{E}) + \mathrm{NPAE}\ \tan(\mathrm{E}) + \mathrm{AN}\ \tan(\mathrm{E})\ \sin(\mathrm{A}) - \mathrm{AW}\ \tan(\mathrm{E})\ \cos(\mathrm{A}) \\ &\quad + \mathrm{WA1}\ \tan(\mathrm{E})\ \sin(2\mathrm{A}) + \mathrm{WA2}\ \tan(\mathrm{E})\ \cos(2\mathrm{A}) + \mathrm{Aobs}\ \sec(\mathrm{E}) \\ \Delta\mathrm{E} &= \mathrm{IE} + \mathrm{GF}\ \cos(\mathrm{E}) + \mathrm{GF2}\ \sin(\mathrm{E}) + \mathrm{AN}\ \cos(\mathrm{A}) + \mathrm{AW}\ \sin(\mathrm{A}) + \mathrm{WA1}\ \cos(2\mathrm{A}) \\ &\quad + \mathrm{WA2}\ \sin(2\mathrm{A}) + \mathrm{R}(\mathrm{Ps}, \mathrm{Ts}, \mathrm{RH}, \mathrm{E}) + \mathrm{ERC}\ \cot(\mathrm{E}) + \mathrm{Eobs}\end{aligned}$$

In the above equation, IA = Az encoder zero offset, CA = Collimation error of RF axis, NPAE = Non-perpendicularity between Az & El axes, AN = Az axis misalignment in N-S, AW = Az axis misalignment in E-W, WA1 & WA2 = Azimuth bearing warp, Aobs = Az pointing offset, IE = El encoder zero offset, GF = Gravitational flexure correction at horizon, GF2 = Gravitational flexure correction for mis-centered EL drive and encoder system, ERC = Empirical correction for atmospheric refraction, Elobs = El pointing offset, and R(Ps,Ts,RH,E) = Refractive index of the atmosphere, where Ps, Ts, and RH = barometric pressure, temperature, and relative humidity, respectively.

Another factor that affects pointing accuracy is the impact of temperature differences in the antenna structure. This factor is challenging to incorporate into a basic pointing model due to its complex nature, which is influenced by variables such as the variance between the sun and antenna orientation, temperature differentials, and other factors. It is known that the temperature difference between the antenna yoke and pedestal has a significant effect on the pointing of the antenna. KVN has designed the antenna in a way that ensures the temperature difference between these parts is maintained below 1 degree (KVN-21M Technical Memo 136, 152). However, actual measurements have shown that the pointing is off by up to 10 seconds per hour during the day when the sun is shining. Therefore, it is necessary to make pointing observations at least every 2 hours during the day, especially at sunrise and sunset, in order to maintain the pointing accuracy at less than 6 arcseconds root mean square.

Since 2009, the telescope's pointing accuracy has been measured using a sample of evolved stars (mainly, 43 GHz SiO maser line). Table 6 presents the pointing accuracy of the four KVN telescopes that were measured in 2025 – 2026. Table 6 provides the total, azimuth, and elevation of the root mean square (rms) of the residual pointing offsets between the observations and the pointing models for each epoch and telescope, accordingly (Total Error = $Sqrt(Az\_Error^2 + El\_Error^2)$. Figure 7 displays the residuals of each KVN telescope's pointing model.

Table 6: KVN Antenna Pointing Accuracy

Site	Total (arcsec)	Azimuth (arcsec)	Elevation (arcsec)	Frequency (GHz)	Date
KYS	**3.78**	2.09	3.15	43	2026-04-22
KUS	**4.33**	2.89	3.22	43	2025-01-27
KTN	**4.61**	2.96	3.53	43	2025-01-24
KPC	**4.10**	2.72	3.07	43	2025-09-23

2.2.6 Beam alignment

The KVN is distinguished by its unique ability to observe a specific target object using four frequency bands simultaneously, a capability unmatched by any other radio observing system in the world. Consequently, the KVN's quasi-optical system must be calibrated so that each of the four beams is directed at the same point in the sky, facilitating simultaneous observation across all four frequency bands. To achieve this, the 86 GHz RCP beam was used

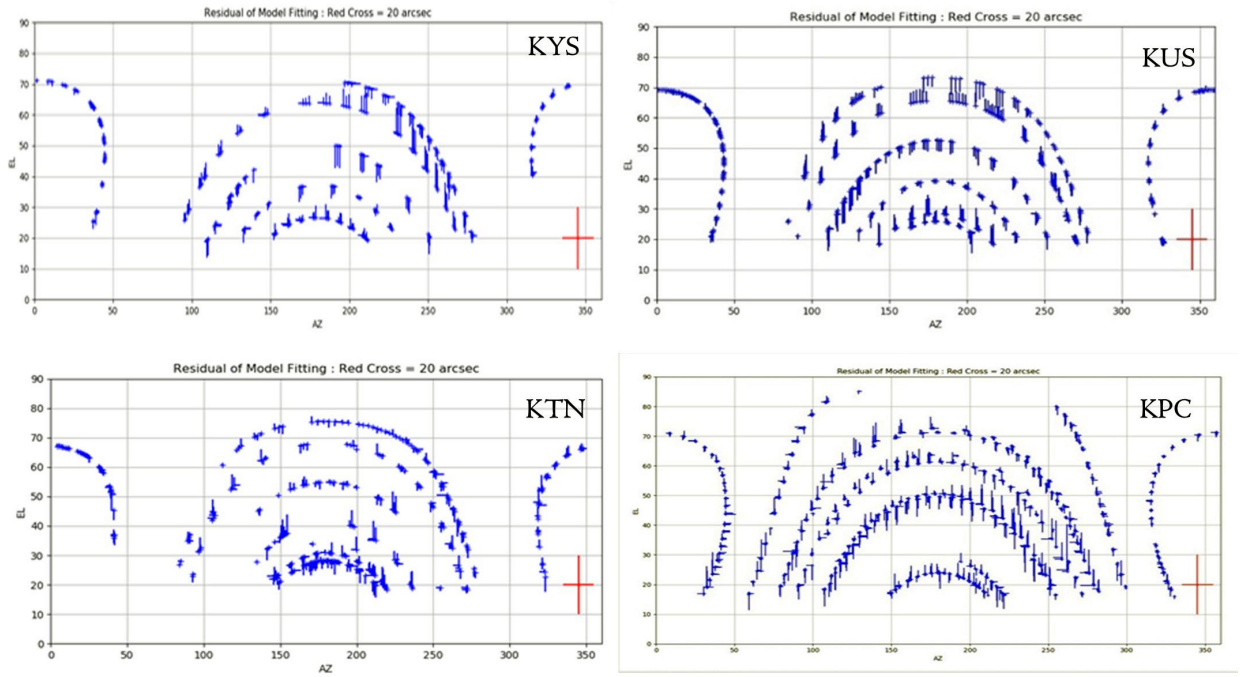

Figure 7: The residual of pointing models (KYS, KUS, KTN, and KPC from top-left to bottom-right).

as a reference point, and the position of the quasi-optical system was adjusted to ensure that the beams of the other frequency bands were properly aligned with its center point. The pointing offset values were subsequently analyzed. For KPC equipped with CTR, since the 150/230 GHz receiver were not yet installed, only the offsets for the 22 and 43 GHz LCP/RCP and the 86 GHz LCP were measured relative to the 86 GHz RCP. The 150/230 GHz receiver is scheduled for installation within 2026. The KYS was also replaced by the CTR, which has the same specifications as the KPC, in April 2026. Therefore, the beam alignment was newly measured as well. The results of this measurement are summarized in Table 7.

2.2.7 Skylines

Skylines are the limits of the viewable height with azimuth below which we cannot see the sky. These limits are determined by obstructions caused by the neighboring buildings, trees, and mountains. Skylines of KVN sites measured in May 2025 are shown in Figure 8.

2.3 Receiver

2.3.1 Quasi-optics

The KVN has the unique capability to observe four frequency bands [4], [5], simultaneously. KVN quasi-optics were designed to enable this multi-frequency observation. Figure 9 shows the layout of quasi-optics and receivers viewing from the sub-reflector side. The quasi-optics system splits one signal from the sub-reflector into four using three dichroic low-pass

Table 7: AZ/EL beam offset with respect to the 86 GHz RCP beam

Site	Band (L, R) (GHz)	Az. offset (arcsec)	El. offset (arcsec)	Measeured Date
KYS	22 (L)	+1.4 (±0.3)	+1.4 (±0.3)	2026-04-21
	22 (R)	+2.1 (±0.8)	+1.0 (±0.6)	2026-04-21
	43 (L)	+1.8 (±0.2)	+1.4 (±0.3)	2026-04-21
	43 (R)	−1.6 (±0.2)	+1.7 (±0.1)	2026-04-21
	86 (L)	−1.7 (±0.2)	−1.3 (±0.6)	2026-04-21
	86 (R)			2026-04-21
	100 (L)	−0.4 (±0.8)	+0.2 (±0.2)	2026-04-21
	100 (R)	+0.6 (±0.8)	+0.5 (±0.8)	2026-04-21
KUS	22 (L)	−1.6 (±0.2)	+2.2 (±0.4)	2025-12-27
	22 (R)	−1.6 (±0.4)	+2.3 (±0.2)	2025-12-27
	43 (L)	+0.3 (±0.1)	−0.4 (±0.2)	2025-12-27
	43 (R)	+1.7 (±0.2)	+0.2 (±0.1)	2025-12-27
	86 (L)	−2.0 (±0.1)	+0.2 (±0.1)	2025-12-27
	86 (R)			2025-12-27
	129 (L)	−1.6 (±0.0)	+0.2 (±0.1)	2025-12-27
	129 (R)	−2.4 (±0.1)	+0.3 (±0.2)	2025-12-27
KTN	22 (L)	−2.0 (±0.2)	−0.7 (±0.4)	2025-12-27
	22 (R)	−2.6 (±0.4)	−0.6 (±0.5)	2025-12-27
	43 (L)	−1.9 (±0.1)	−1.8 (±0.1)	2025-12-27
	43 (R)	−2.0 (±0.2)	−1.1 (±0.2)	2025-12-27
	86 (L)	−2.0 (±0.1)	+0.3 (±0.1)	2025-12-27
	86 (R)			2025-12-27
	129 (L)	−0.1 (±0.1)	−0.6 (±0.1)	2025-12-27
	129 (R)	−1.4 (±0.1)	−0.7 (±0.1)	2025-12-27
KPC	22 (L)	+2.4 (±0.5)	+2.3 (±0.6)	2026-01-08
	22 (R)	+1.7 (±0.1)	+2.4 (±0.1)	2026-01-08
	43 (L)	−0.2 (±0.1)	−0.2 (±0.1)	2026-01-08
	43 (R)	−3.2 (±0.1)	0.0 (±0.1)	2026-01-08
	86 (L)	−1.1 (±0.0)	0.0 (±0.1)	2026-01-08
	86 (R)			2026-01-08
	100 (L)	−1.5 (±0.1)	+1.8 (±0.1)	2026-05-08
	100 (R)	−0.6 (±0.1)	+1.3 (±0.1)	2026-05-08

filters marked as LPF1, LPF2, and LPF3 in Figure 9. The split signals into four different frequency bands are guided to corresponding receivers.

In 2018, KVN developed a Compact Triple-band Receiver (CTR) system that integrates three frequency bands: 22 GHz, 43 GHz, and 86 GHz. By accommodating these three bands within a single cryogenic chamber, the system not only reduces the space required compared to existing KVN multi-channel receiving systems but also improves maintenance convenience. Figure 10 illustrates the quasi-optical configuration of the CTR system, which includes two

Figure 8: Skylines of KYS, KUS, KTN, and KPC from top to bottom.

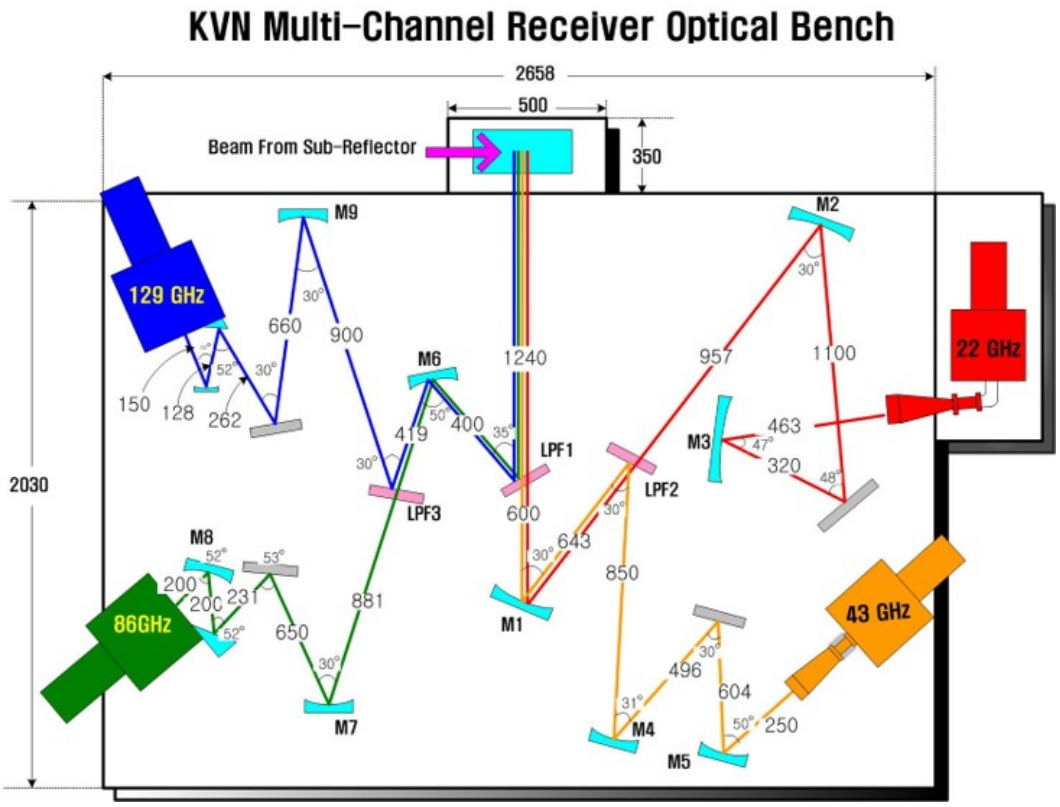

Figure 9: KVN multi-frequency receiving system.

low-pass filters (LPF1 and LPF2). For reference, the CTR was installed at KPC in January 2024, and in April 2026, the existing KVN multi-frequency receiving system at KYS was also upgraded to the CTR.

In mid-2023, the construction of the KPC was completed. The receiving system of the KPC has been developed as an compact and wide-band receiver capable of simultaneous observations in the 18−230 GHz band. For the K, Q, and W bands, the CTR was designed and manufactured in-house to simultaneously observe them. To be more specific, the CTR system is mainly composed of a quasi-optical circuit, a cryogenic receiver, and a room temperature receiver system. The receiving frequency bands are divided into K (18–26 GHz), Q (35–50 GHz), and W band (80–116 GHz). These RF signals are then amplified and down-converted in the room temperature receiver, and finally converted into IF signals of 8–16 GHz. Additionally, it is possible to observe two polarization components (LCP and RCP) for each band simultaneously.

The quasi-optical circuit is a critical component that allows for simultaneous three-channel observations. It determines the antenna efficiency and receiver noise temperature, requiring complex design and high-quality assembly. Additionally, it necessitates sophisticated receiving beam alignment and precise measurement techniques. Cryogenic receiving systems are designed with a chamber that maintains a high vacuum and cryogenic temperature below 20 K. The chamber is equipped with a feed system that includes a cryogenic Low Noise Amplifier (LNA), feed horn, phase shifter, and orthogonal mode transducer (OMT). These components play a crucial role in influencing the receiver's noise temperature and

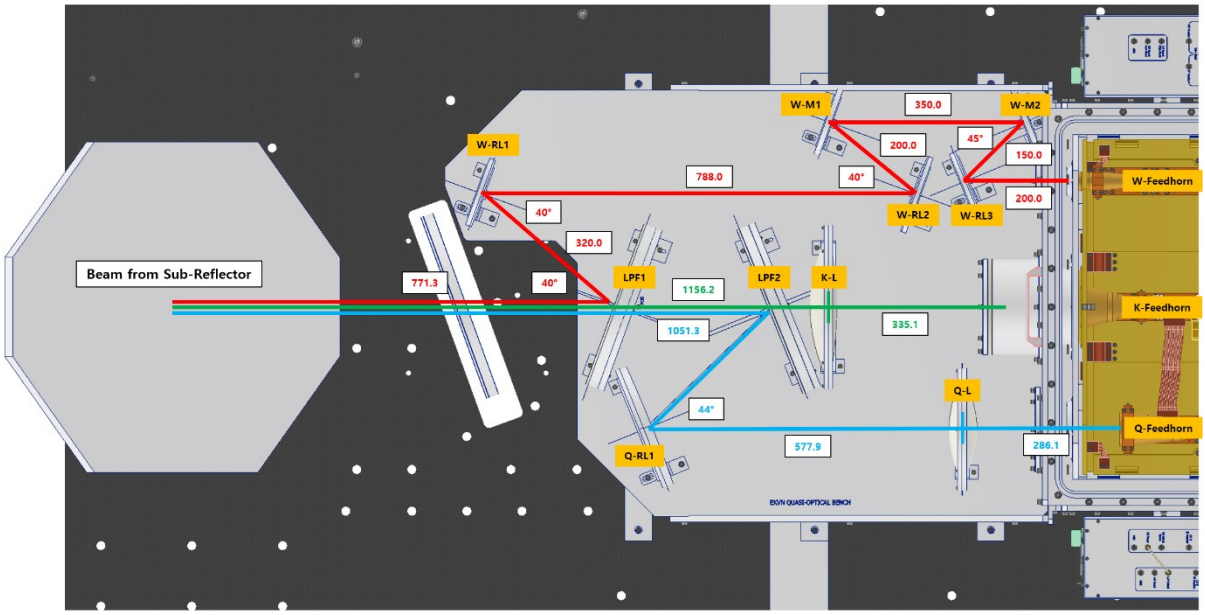

Figure 10: KVN Compact triple-band receiving system.

stability. The room temperature receiving system comprises a room temperature amplifier and a local oscillator (LO) that convert the received RF signal to an intermediate frequency (IF). It also includes several band pass filters (BPFs), power divider, and mixers.

The CX/Ka band receivers were successfully installed on the KPC at the end of April 2025 and are currently undergoing a series of performance tests. Additionally, the 150/230 GHz receivers are scheduled for installation in 2026, with these receivers set to be utilized for research observations starting in 2027. Therefore, performance parameters for these receivers will be updated in next year's status report.

Figure 11 presents a layout of the KPC receivers, while Figure 12 shows a photograph of the receiver room as of May 2025, illustrating the installation of the CTR and CX/Ka band receivers.

2.3.2 Block diagram

The K, Q, and W band receivers are cooled HEMT receivers, while the D band receiver is an SIS mixer receiver [5]. All receivers are capable of receiving dual circular-polarization signals. Among eight signals (four dual-polarization signals), four signals selected by the IF selector are down-converted to the input frequency band of the sampler. The samplers digitize signals into 2-bit data streams with four quantization levels. The sampling rate is 1024 Mega samples per second, resulting in a 2 Gbps data rate (2-bit $\times$ 1024 megabytes per second) and 512 MHz frequency bandwidth. In total, we can get 4 streams of 512 MHz bandwidth (2 Gbps data rate) simultaneously, which means that the total rate is 8 Gbps.

New wide-band VLBI backends, including OCTAD, Mark 6, and GPU spectrometers, were installed for wide-band operation. They are indicated in the red box of Figure 13. The OCTAD consists of four analog-to-digital converters, digital signal processing modules, and a VDIF formatter. It digitizes four IF signals and performs signal processing for digital down-

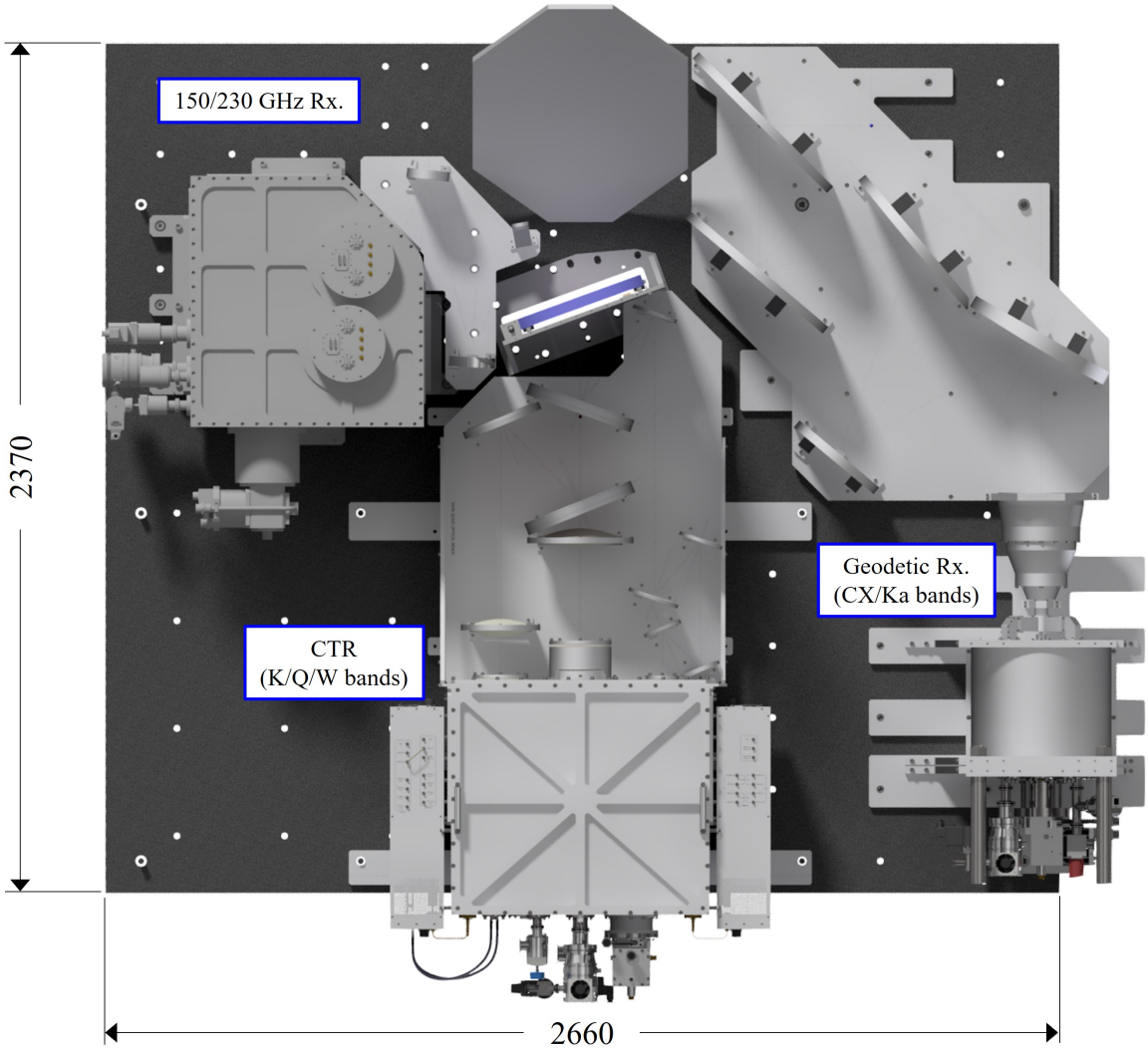

Figure 11: Layout of the KPC receiving system.

conversion and filtering. Combining OCTAD and ADS1K+Fila10G, all eight IF signals (four dual-polarization signals) can be obtained at the same time. The OCTAD has four 10 GbE outputs, with which we can get a maximum 32 Gbps aggregated data rate.

Furthermore, two wide-band VLBI sampler OCTADs and two GPU spectrometers were installed at KPC withe the objective of achieving enhanced performance in comparison to the original KVN system. As a result, the output rate of the KPC OCTAD can reach up to 64 Gbps. The details of the backend system, including OCTAD, are introduced in Section 2.4. The block diagram of receivers and backend interface of the KPC are illustrated in Figure 14.

2.3.3 Frequency range

The instantaneous bandwidth of the 1st IF of each receiver is limited to 8 GHz by the band-pass filter. Table 8 shows the frequency range of each receiver. The Q and W bands

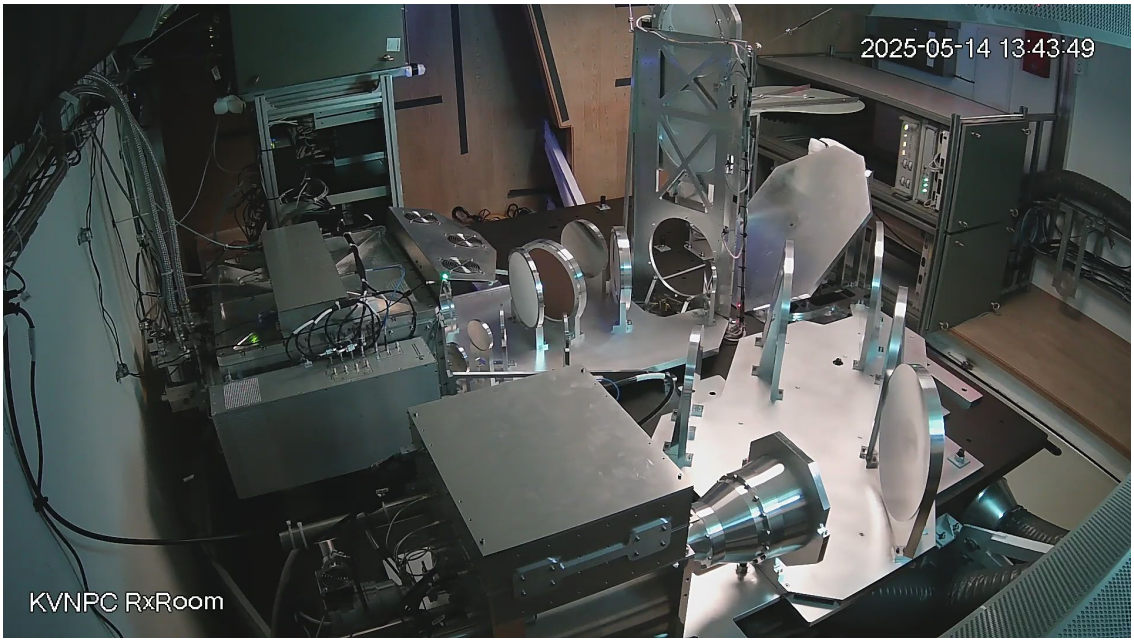

Figure 12: Receivers installed at KPC as of May 2025 (CTR + C/X/Ka band receivers).

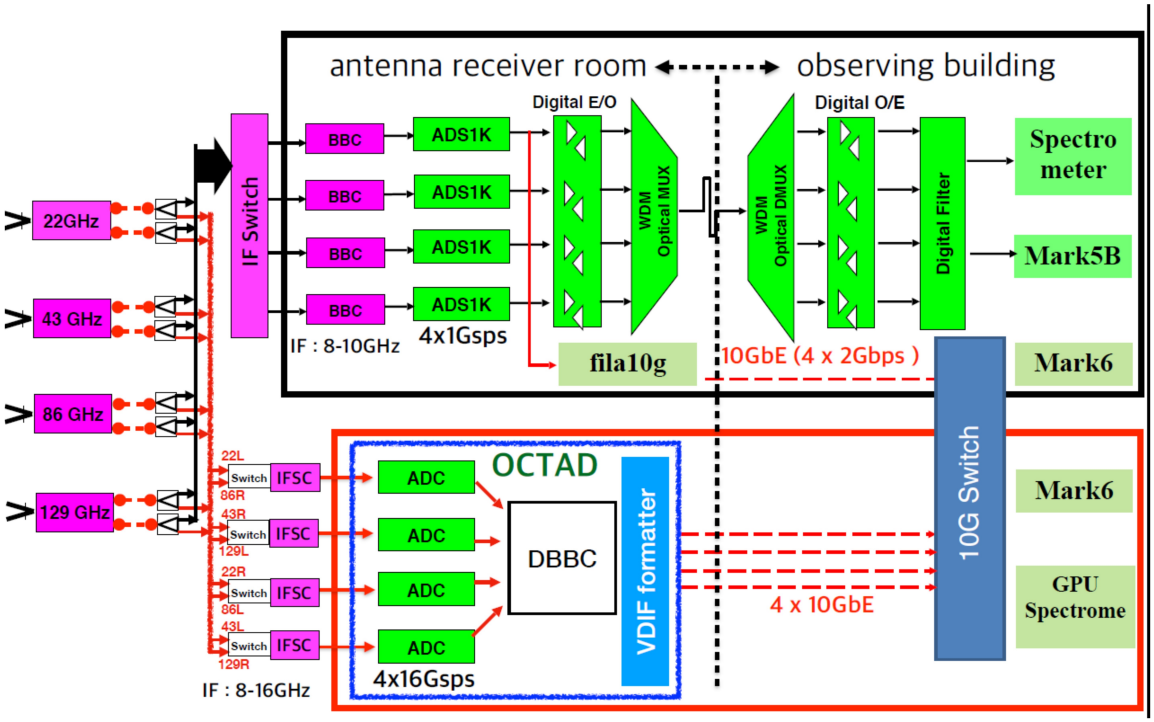

Figure 13: KVN signal flows including a new wide-band sampler OCTAD (from 2020).

are divided into two frequency blocks. The low (high) frequency ranges of the Q band receiver are from 35 (42) to 42 (50) GHz. The low (high) frequency ranges of the W band receiver are from 85 (100) to 99 (116) GHz. Low- and high-frequency bands of the same polarization cannot be observed at the same time. Note that the D band receiver has 2 GHz

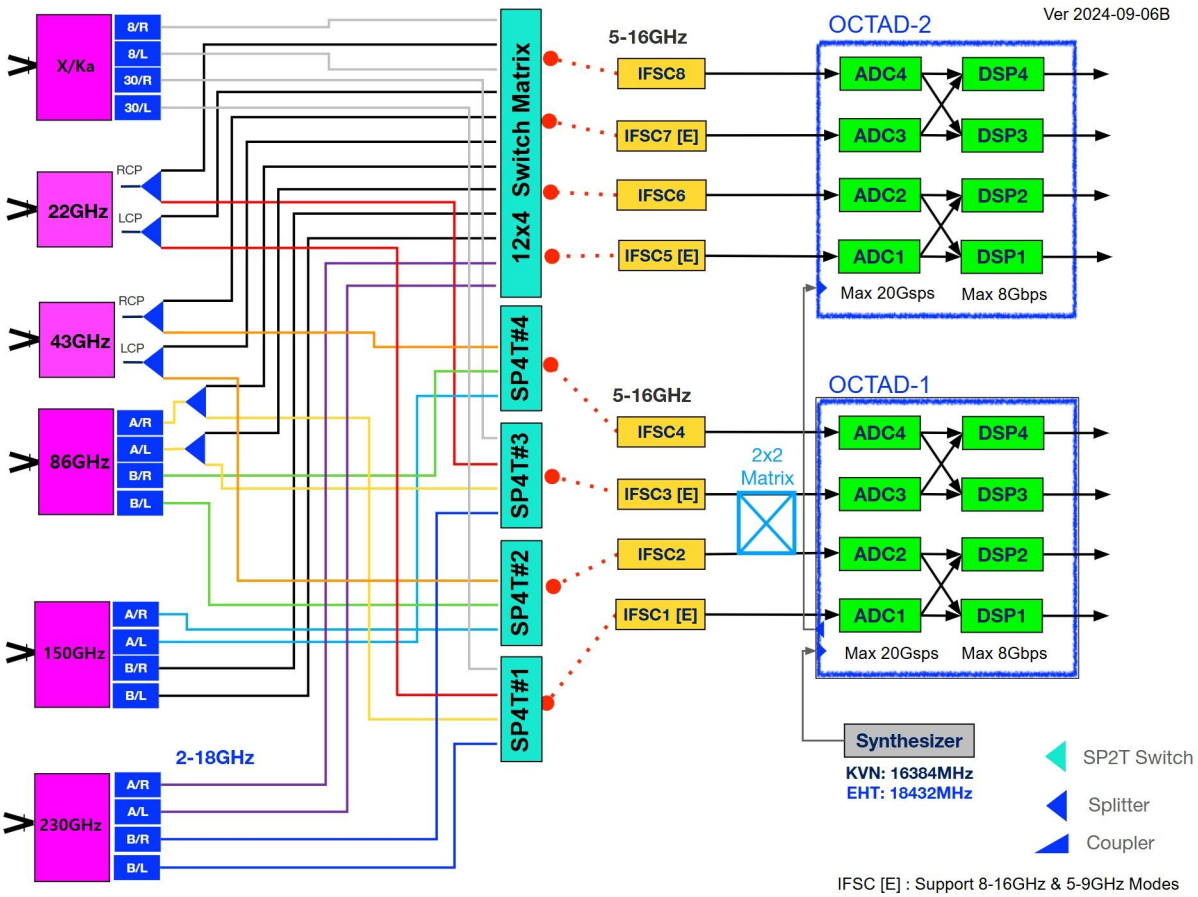

Figure 14: Block diagram of the signal connection between receivers and backend interface of the KPC.

IF bandwidth. The KPC with CTR system has slightly different frequency bands than the original KVN receivers. In the future, all original KVN receivers will be replaced with the CTR system.

2.3.4 Receiver noise temperature

Every frequency band has a receiver noise temperature that ranges from roughly 50 to 80 K. These values are similar for all bands. The loss of quasi-optics does not reduce the efficiency of the antenna aperture since the calibration chopper is placed before the quasi-optics; rather, it raises the temperature of the receiver noise. As a result, 40–50 K are added to the noise temperatures to account for the quasi-optics losses.

2.3.5 System temperatures with wide-band frequencies

Wide-band observations are now possible with the KVN thanks to the integration of the GPU spectrometer and a new backend (OCTAD). In this regard, we evaluated the system temperatures over all wide-band frequency ranges, and the results are presented in Table 9.

Table 8: Frequency range of the KVN receiver

Band	Frequency range (GHz)	Telescope
CX	6 – 9	KUS, KPC
Ka	28 – 34	KPC
K	18 – 26	KYS, KUS, KTN, KPC
Q-low	35 – 42	KYS, KUS, KTN, KPC
Q-high	42 – 50	KYS, KUS, KTN, KPC
W-low	85 – 99	KUS, KTN
W-low	80 – 99	KYS, KPC
W-high	99 – 116	KYS, KUS, KTN, KPC
D	125 – 142	KUS, KTN
D-wide	125 – 175	KYS, KPC (in prep.)
sub-mm	210 – 275	KYS, KPC (in prep.)

As a sample result, Figure 15 shows the system temperatures measured for the KTN's wide-band receiver system.

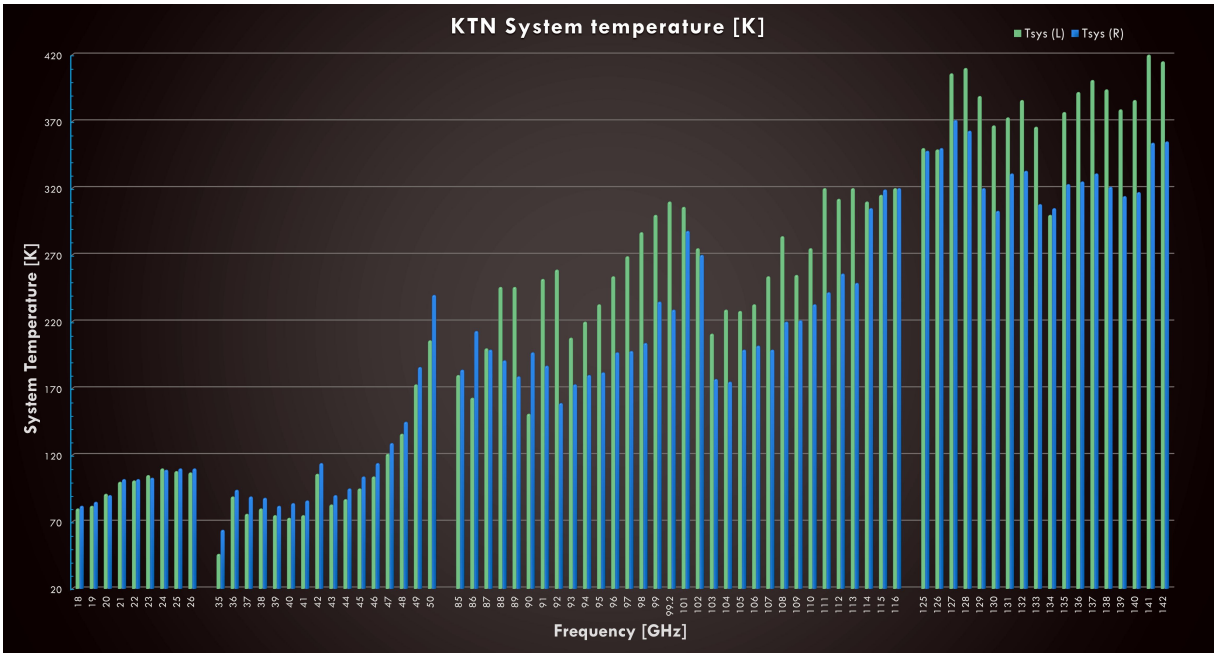

Figure 15: System temperatures with all wide-band frequencies of the KTN.

2.4 Backend/Digital Process

The KVN backend comprises (wide-band) samplers that convert the IF signal from the receiver into a digital signal and (wide-band) high-speed recorders that transfer the signal from the sampler to the hard disk. The KVN has used two types of data acquisition systems:

Table 9: System temperatures ($T_{\rm sys}$) using wide-band frequencies

Site	Band	Freq. range (GHz)	$T_{\rm sys}$ (K)	El. (degree)	Date
KYS	K	18 – 26	82 – 98	45 – 49	Jan. 17, 2023
	Q-low	35 – 42	60 – 112	51 – 52	Jan. 17, 2023
	Q-high	43 – 50	91 – 140	45 – 48	Jan. 17, 2023
	W-low	85 – 100	147 – 191	59 – 65	Jan. 27, 2023
	W-high	101 – 116	131 – 255	40 – 43	Feb. 01, 2023
	D	125 – 142	139 – 180	35 – 51	Jan. 27, 2023
KUS	K	18 – 26	71 – 91	55 – 56	Feb. 08, 2023
	Q-low	35 – 42	51 – 118	51 – 52	Feb. 08, 2023
	Q-high	43 – 50	85 – 156	46 – 48	Feb. 08, 2023
	W-low	85 – 100	153 – 203	48 – 61	Feb. 08, 2023
	W-high	101 – 116	150 – 315	43 – 61	Feb. 10, 2023
	D	125 – 142	145 – 279	36 – 46	Feb. 08, 2023
KTN	K	18 – 26	80 – 110	59 – 62	Nov. 10, 2024
	Q-low	35 – 42	46 – 114	49 – 58	Oct. 15, 2024
	Q-high	43 – 50	83 – 240	58 – 59	Oct. 15, 2024
	W-low	85 – 100	150 – 310	59 – 65	Oct. 19, 2024
	W-high	101 – 116	175 – 320	57 – 63	Oct. 20, 2024
	D	125 – 142	300 – 420	37 – 48	Oct. 27, 2024
KPC	K	18 – 26	54 – 83	34 – 62	Apr. 30, 2025
	Q-low	35 – 42	54 – 100	66 – 74	Apr. 30, 2025
	Q-high	43 – 50	101 – 200	51 – 58	Apr. 30, 2025
	W-low	80 – 97	148 – 191	34 – 64	May 02, 2025
	W-high	98 – 116	117 – 450	43 – 70	May 12, 2025

DAS and OCTAD. The old legacy system, DAS is replaced by another OCTAD during the summer maintenance season in 2026, and new recorders are introduced to standardize the digital backends across all KVN systems. The old legacy DAS will no longer be available from 2026B, resulting in changes to the available modes for both VLBI and single-dish observations.

2.4.1 Signal processing mode of OCTAD

The OCTAD (Optically Connected Transmission system for Analog to Digital Conversion) is the second-generation data acquisition system of KVN. It consists of four high-speed samplers, four DSP modules, and one VDIF formatter, as illustrated in Figure 16. The system accepts four IF signals, quantized them to a resolution of up to 3 bits, and generates digital output data transmitted over fiber optic cables. Each unit has a standard data transfer capability of 10 Gigabit Ethernet (GbE).

The OCTAD enables us to select in the frequency domain a maximum of 16 data streams from 4 streams of 8192 MHz bandwidth. The maximum output rate is 32 Gbps (4×8 Gbps)

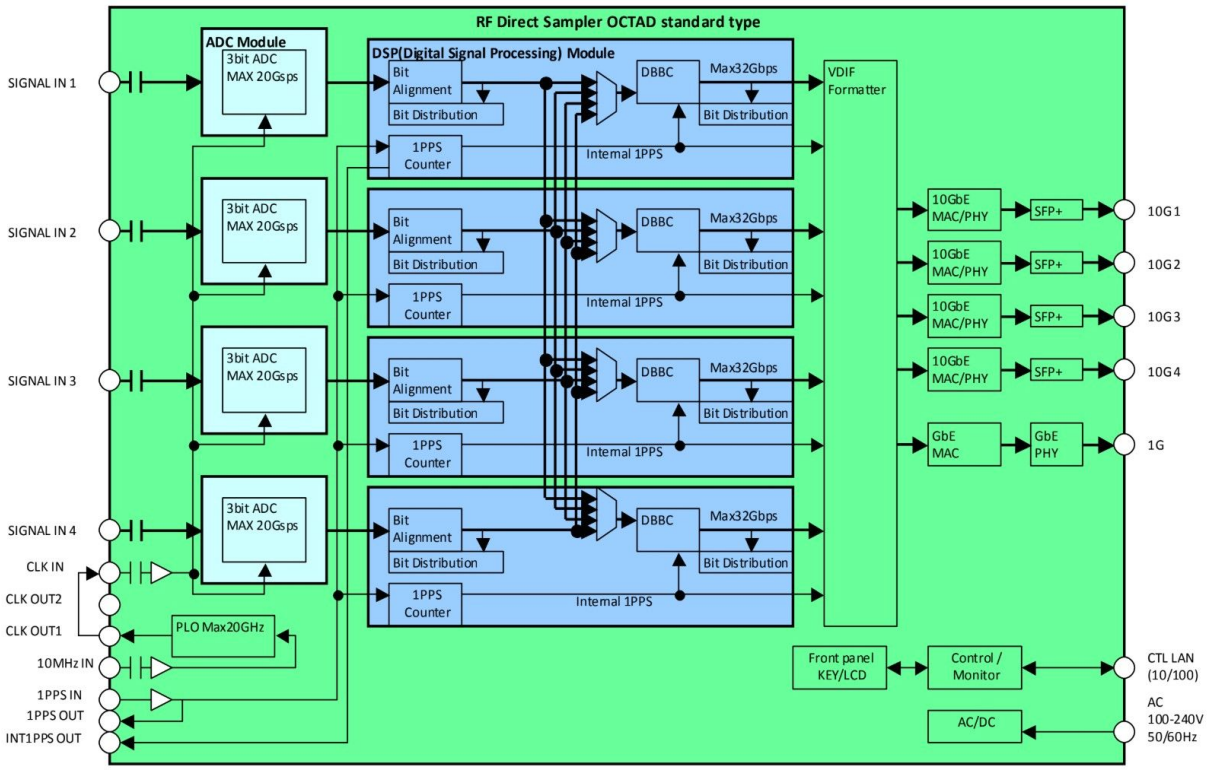

Figure 16: Functional Block diagram of the OCTAD

Table 10: KVN OCTAD mode

Bandwidth (MHz)	Max. Number of streams	Total data rate (Gbps)
16	16	1
32	16	2
64	16	4
128	16	8
256	16	16
512	16	32
1024	8	32
2048	4	32

of which the net bandwidth is 8 GHz (4×2 GHz bandwidth). The total aggregated bit rate, number of streams, and bandwidths are specified in Table 10. The output data stream from the signal processing unit is routed to the VDIF formatter, which converts the output of the DBBC to the specified data format. The final formatted data are then converted to optical data and transmitted to the recorder unit using a standard communication protocol called 10 GbE.

Meanwhile, as mentioned above, the legacy system DAS will be terminated and replaced with another OCTAD, and all KVN telescopes will have two OCTADs from 2026B. As a

result, the maximum output rate reachs 64 Gbps, which corresponds to 16 GHz aggregated bandwidth for 2-bit sampled data. Notably, this enhancement aligns the KVN with the observing mode specifications (2 GHz × 4 IF × 2 pol.) of the Event Horizon Telescope (EHT).

2.4.2 Recorders

The KVN station currently employs two main recording systems: the Mark6 and the Flexbuff.

Mark6 is a hard disk recording system developed at Haystack Observatory, USA. It supports a maximum data rate of 32 Gbps. For more details, see Haystack-memo-MK6. The Mark6 records OCTAD outputs in VDIF (VLBI Data Interchange Format), offering greater flexibility in terms of IF numbers and bandwidth. The DAS and Mark5B systems, which were used for EAVN 6.7 GHz observations, have been retired and replaced by the OCTAD and Mark6 starting from the 2026B season.

Since 2023, we have adopted **Flexbuff**, a system for recording VLBI data at ultra-high speeds, developed by JIVE and proven for its performance and reliability by EVN and other networks (see Figure 17). The Flexbuff system comprises a single host-based hardware unit that integrates more than 32 HDD arrays and storage servers to accommodate high-volume, high-bandwidth files, along with software that supports data recording at 32 Gbps. Due to the absence of dedicated hardware for producing Flexbuff, the KVN selected PCI-E 4.0 and a 3rd-generation CPU to handle the four 8 Gbps streams output from the OCTAD in real time. The Flexbuff platform, based on the "Supermicro" model, has been installed at all KVN sites. Additionally, **jive5ab**–a copy manager software designed for recording and transmitting VLBI data and based on the Linux OS "Rocky"–has also been installed.

2.4.3 GPU Spectrometers for Single-dish observation

The GPU Spectrometer (GSM) processes VDIF data streams from OCTAD to generate power spectra using FFT computations. The maximum data processing rate of the GSM is 32 Gbps with the current KVN GSM configuration. The number of available streams depends on the OCTAD setup. Since one OCTAD can process a maximum of 16 streams, the maximum number of streams from two OCTADs is 32 for bandwidths up to 256 MHz. However, this number decreases for wider bandwidth modes due to the 32 Gbps data rate limitation. Table 11 summarizes these details. The maximum number of FFT points per stream is 8192. The instantaneous frequency range of each ADC is 8192–16384 MHz. Excluding approximately 200 MHz at the band edges, where calibration accuracy is poor, the maximum frequency span across streams within the same IF should be less than **7.8 GHz**. For example, it is possible to observe $C^{18}O$ $J = 1 - 0$ at 109.782 GHz, ^{13}CO $J = 1 - 0$ at 110.201 GHz, CN $1 - 0$ at 113.491 GHz, and ^{12}CO $J = 1 - 0$ at 115.271 GHz simultaneously from one IF. However, SiO $J = 2 - 1$ at 86.243 GHz and CH_3OH at 95.169 GHz cannot be observed simultaneously within a single IF.

The GSM can generate both auto- and cross-power spectrum data. Single-dish polarization observations are valuable not only for the results obtained from these observations but also as a crucial component for calibrating polarization angles in VLBI. Accordingly, a polarization observation mode for the KVN was developed using the wide-band backend system

Figure 17: Front view of the two Flexbuff units at KPC. 24 disks are mounted for one Flexbuff.

OCTAD and the GSM. Figure 18 shows the sample results from polarization observations. For the cross-correlation process with the current KVN GSM, both polarization data must be included in a single 10 GbE output. Since the 2048 MHz bandwidth mode requires two 10 GbE outputs, note that the legacy FX-type digital spectrometer (DSM), which processes data streams from the legacy DAS, will no longer be available starting from 2026B.

2.4.4 Correlator

- **Daejeon Correlator in KJCC**
  KJCC(Korea-Japan Correlation Center) gathers the raw VLBI observation data from each site of KVN, VERA/JVN, and CVN, and performs the correlation process with two VLBI correlators. The first one, Daejeon Correlator, is one of the fastest VLBI correlators in the world and is used for processing the KaVA and EAVN observations mainly. It is capable to correlate the data streams of max. 8 Gbps for max. 16 stations in one pass, to produce the correlated output of 8192 spectral points for each sub-bands. The number of spectral points is reduced to 128 for continuum, 512 for line observation after the correlation process by channel integration.

  For the final correlation output, the default accumulation time is 1.6384 seconds and the final frequency resolutions are 16–128 MHz for continuum observations, and 16–512 MHz for line observations in default.

Table 11: Available mode of the GPU spectrometer (GSM)

Bandwidth (MHz)	Number of streams	Total data rate (Gbps)	Polarization Mode
32	32	4	Y
64	32	8	Y
128	32	16	Y
256	32	32	Y
512	16	32	Y
1024	8	32	Y
2048	4	32	Y

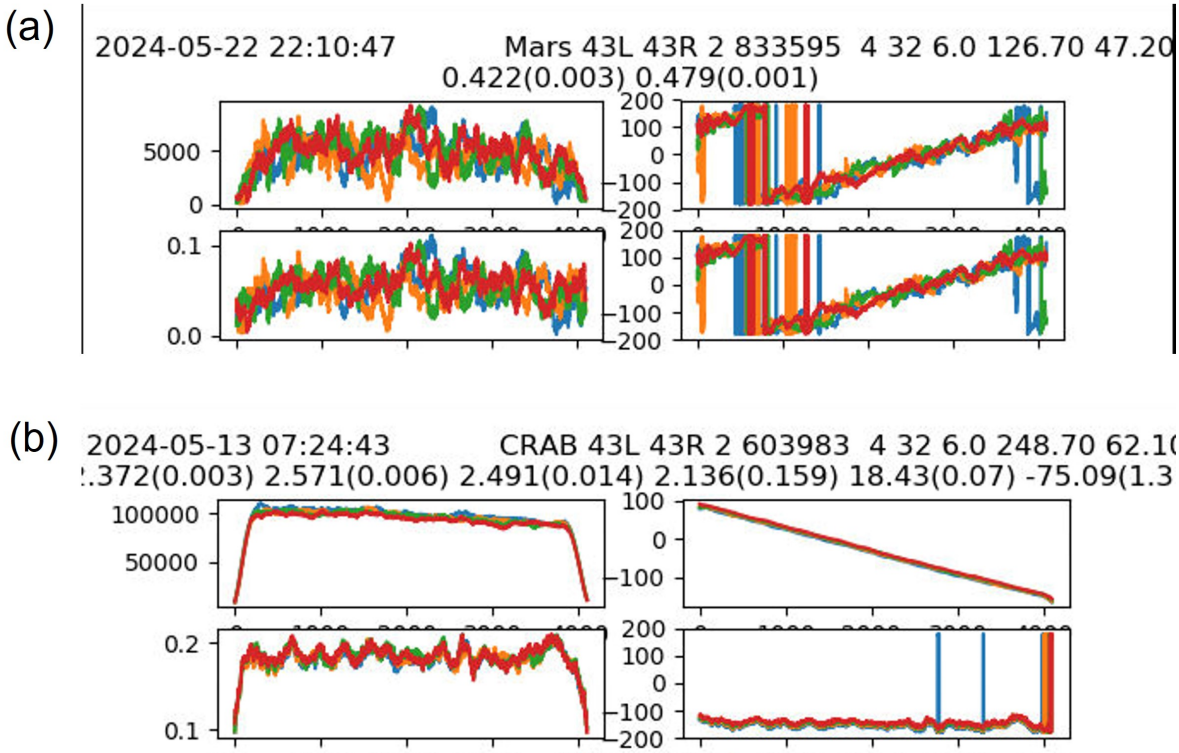

Figure 18: (a) The spectral result of a planet 'Mars' for calibration of polarization (left: amplitude, right: phase): Column 1 and 2 show the measurement and D-term, respectively. (b) Spectra of the polarization angle-corrected source 'CRAB' utilizing GSM (left, right: same as above): column 1 and 2 show the measured values and the linear polarization results.

The KJCC is currently able to support the following correlation modes (see Table 12).

The KJCC supports the following number of frequency channels for preparing FITS file.

- Basic output channel of correlator: 8192 frequency channel
- Continuum: 128 frequency channel (64 channels integrated in post-correlation)

– Spectral line: 512 frequency channel (16 channels integrated in post-correlation)

Correlation processing will take about 1 week to prepare the first version of FITS after the data arrives from the last station. However, the KJCC team will do their best to make correlation results available as quickly as possible to deliver the FITS file to PI. For more details, please see the webpage KJCC.

- **Software Correlator, DiFX**
  The second one, DiFX (Distributed FX-style) software correlator (see Deller et al. (2007 [6], 2011 [7]), is a widely used and well-established software correlator and is utilized for processing KVN observations. It provides highly flexible correlation modes, allowing users to specify accumulation time and frequency resolution appropriate for their scientific objectives.

  A dedicated high-performance computing cluster is used for software correlation. It consists of a master node and multiple computing nodes. The system has recently been upgraded to a modern CPU architecture based on AMD EPYC processors. The computing nodes are equipped with dual-socket AMD EPYC 9654 processors. Each processor has 96 cores, resulting in a total of 192 cores per node. The nodes operate with single-threaded cores (one thread per core) to optimize performance for parallel correlation tasks. Each node has approximately 512 GB of memory and is configured with a NUMA architecture consisting of two nodes. The processors support advanced vector instructions including AVX-512, which significantly improves FFT and cross-correlation performance. The master node is responsible for job control, correlation parameter configuration, and data management, while the computing nodes perform the FFT (F-stage) and cross-multiplication (X-stage) processes of the DiFX correlator using MPI-based parallel computation. The master and computing nodes are connected through a high-speed Infiniband network (≥ 100 Gbps), which is used for parallel computation and data transfer. A secondary Ethernet network is used for system management and monitoring.

  A dedicated Lustre parallel file system is used for software correlation, providing multi-petabyte-scale storage. The file system is connected to all nodes through the

Table 12: Correlation mode of the KJCC

Obs. Mode	Total Data Rate	Bandwidth /sub-band	# of sub-bands	Minimum Accum. Time	# of Freq. Channels /sub-band
C5	1024 Mbps	16 MHz	16	1.6384 sec	8192
C4	1024 Mbps	32 MHz	8	0.8192 sec	8192
C3	1024 Mbps	64 MHz	4	0.4096 sec	8192
C2	1024 Mbps	128 MHz	2	0.2048 sec	8192
C1	1024 Mbps	256 MHz	1	0.1024 sec	8192
W1	2048 Mbps	512 MHz	1	0.0512 sec	8192
W2	4096 Mbps	512 MHz	2	0.0512 sec	8192
W4	8192 Mbps	512 MHz	4	0.0512 sec	8192

Infiniband network, enabling high-throughput parallel I/O required for VLBI data processing.

Observation data recorded in Mark6 and the FlexBuff at each KVN site are transferred to the Lustre file system via the KREONET using high-speed data transfer protocols such as GridFTP or Globus. The master node is connected to KREONET via high-speed Ethernet, allowing efficient data ingestion. The KYS, KUS, KTN, and KPC sites are connected to KREONET via 100 Gbps networks. The upgraded computing infrastructure significantly enhances the performance of the DiFX correlator, enabling higher frequency resolution, longer integration times, and efficient processing of large-scale VLBI datasets. Figure 19 shows the Coma computing cluster and the Lustre file system.

Technical details of the software correlator are described in the homepage DiFX.

- **GPU based Correlator, Halcyon**
  The third one, Halcyon, is the first GPU-based, FX-style correlator developed by KASI's correlator team. The Halcyon correlator was implemented in C++ to optimize the utilization of GPU CUDA cores. Its short-term objective is to perform real-time correlation processing of 32 Gbps observational data from five stations – including the Sejong station, currently operated for geodetic purposes alongside the four KVN stations – forming 10 baselines with dual polarization. It employs RDMA (Remote Direct Memory Access) over a RoCE v2 network protocol to enable efficient access to data recorded on Flexbuff servers, Mark6 systems, and general-purpose storage. The correlator supports various DAS (Data Acquisition System) formats used in the EAVN (East Asian VLBI Network), including KVN VDIF, VERA/JVN No-Head, CVN DBBC3, and Mark5b, and is capable of processing correlation data from more than 10 stations with dual polarization.

  By leveraging the RoCE v2 network protocol, the system supports remote correlation processing, enabling the correlator at the correlation center to directly read and process observational data stored in remote recorders without transferring the data from the stations to the correlation center (see Figure 20).

  The validation of correlation data processed with Halcyon was conducted by comparing it with results from the DiFX correlator using AIPS. The first stage of validation involved verifying that observation – related information-such as experiment name, observation time, and frequency – matched between the datasets produced by the two correlators. In the second stage, basic calibration through fringe fitting was performed, followed by a comparison of parameters such as SNR and delay derived from the results. The correlation outputs exhibited similar time-dependent variation patterns to those of DiFX, and the SNR values were nearly identical (within approximately 1 %). Therefore, EVN session data observed at 22 GHz in 2 Gbps wideband dual-polarization mode were used to further compare the results of the two correlators (see Figure 21).

  In addition, the final spectral shape – after applying both fringe fitting and bandpass calibration – was examined. Here, too, the results from the two correlators are nearly identical, displaying completely overlapping profiles (see Figure 22).

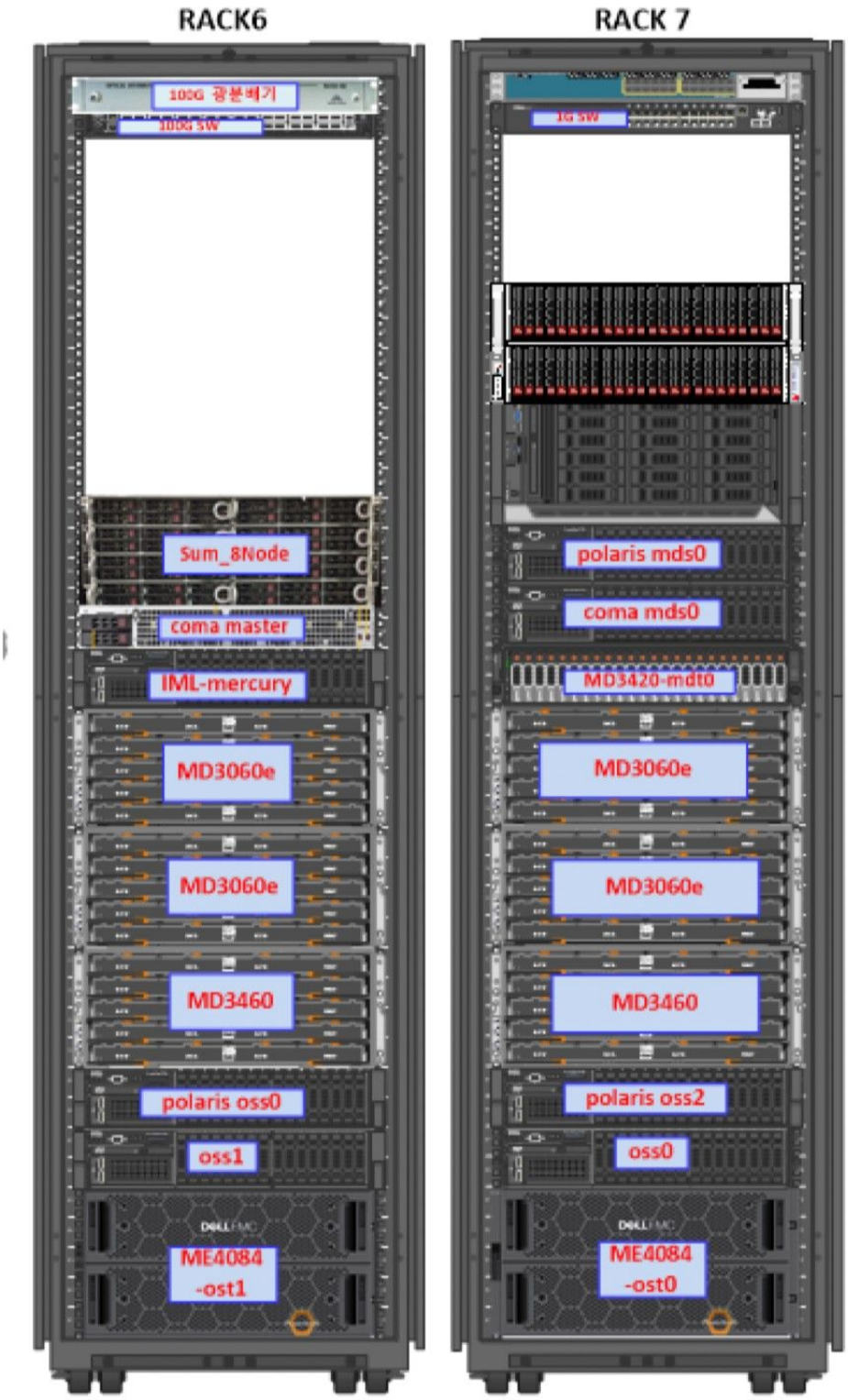

Figure 19: A computing cluster and Lustre file system dedicated for the software correlation of the KVN.

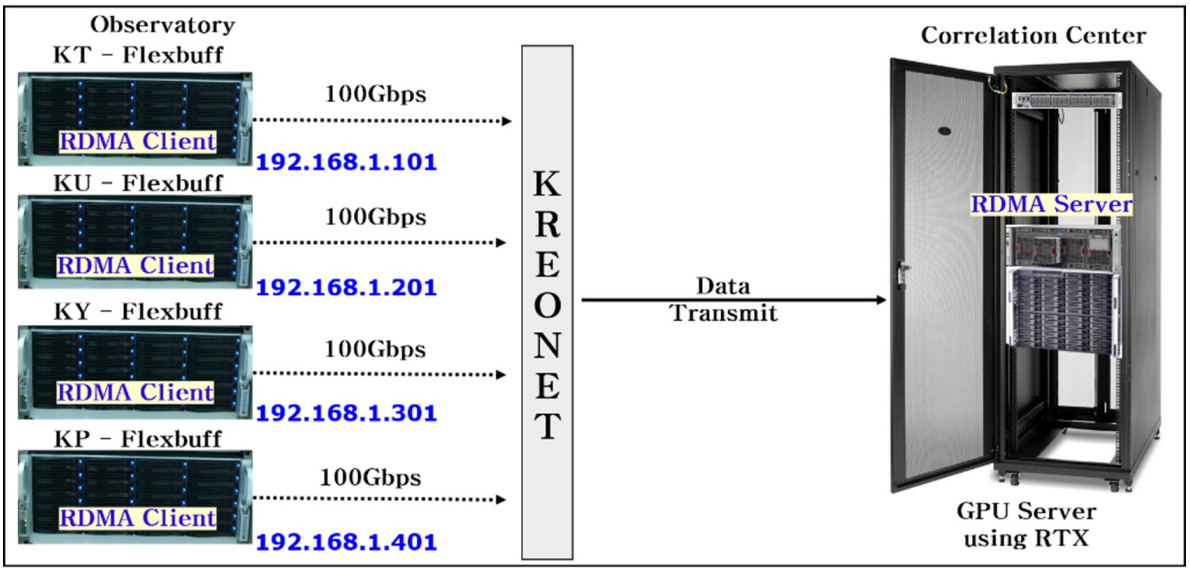

Figure 20: Remote correlation concept for Halcyon correlator.

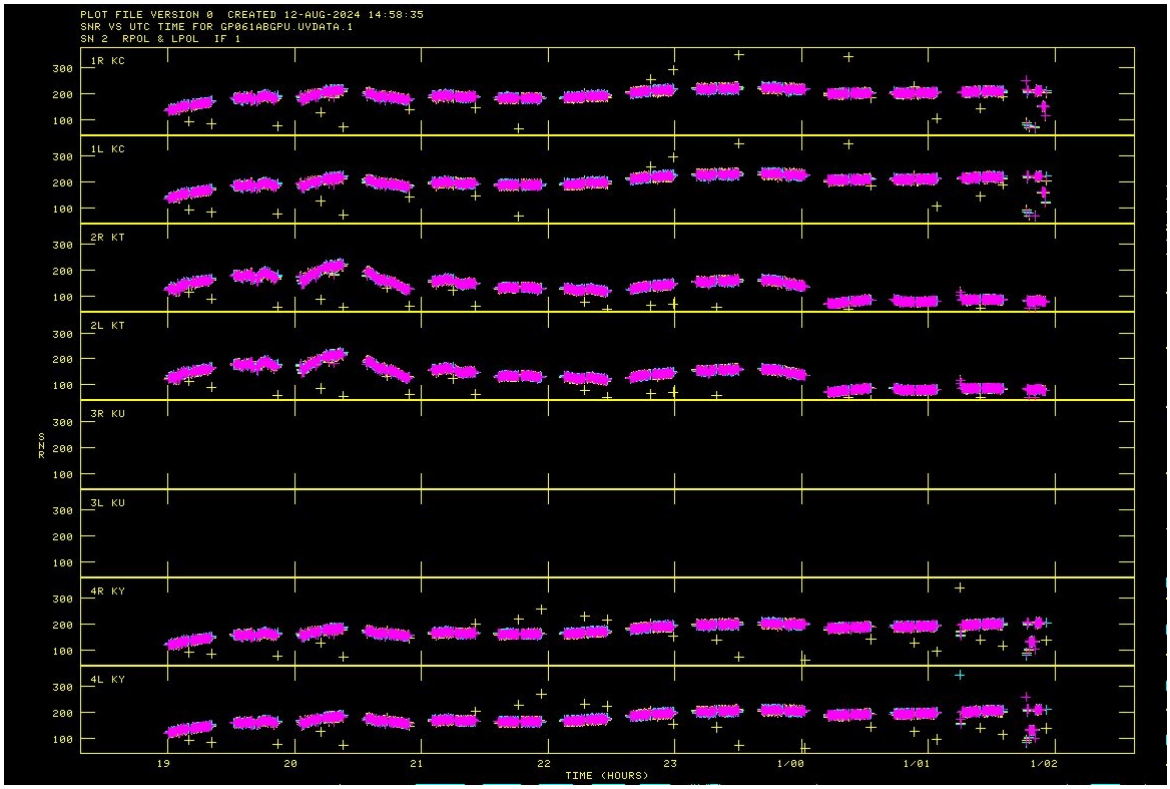

Figure 21: SNR variation pattern after fringe fitting. The results from DiFX (blue) and Halcyon (yellow) are displayed, with most values overlapping and appearing purple, indicating a high degree of similarity.

- **FITS delivery**
  Correlations will be performed using either the DiFX or the Daejeon correlator. The

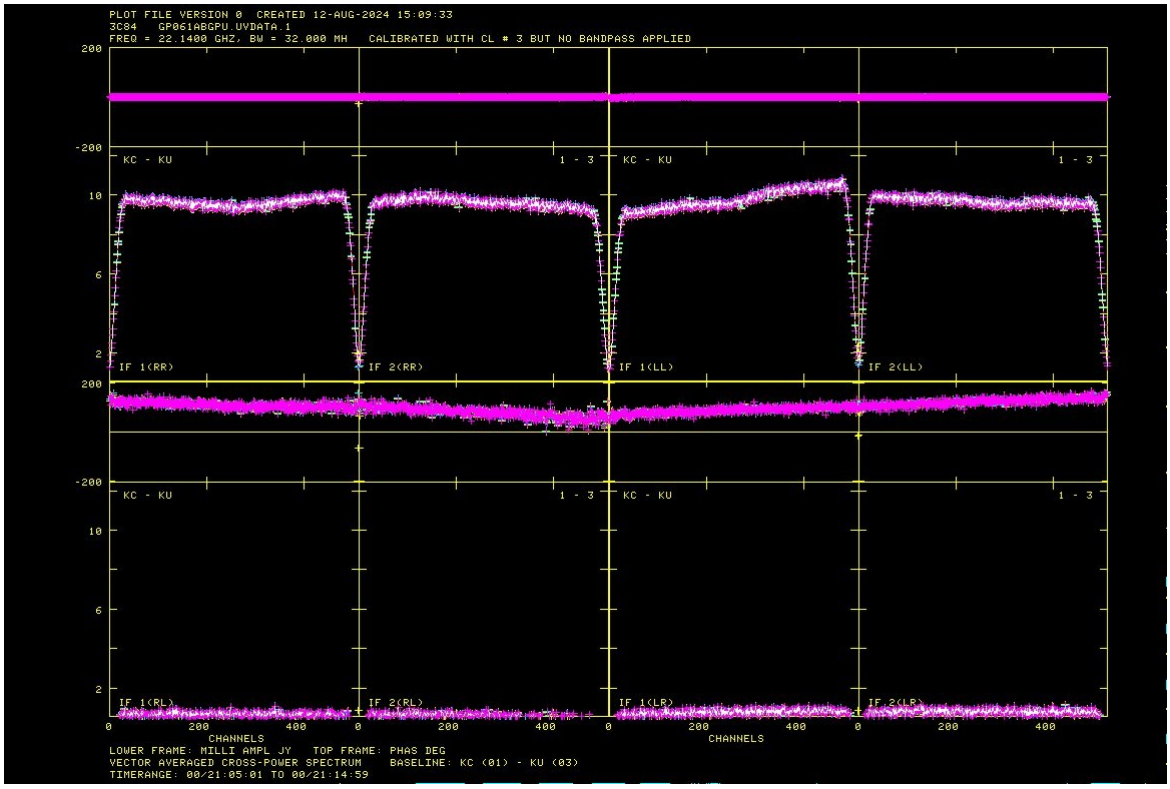

Figure 22: Spectral shape of the continuum source 3C84 after applying all calibrations. The results from DiFX (blue) and Halcyon (yellow) are shown; most values overlap, appearing purple, which indicates that the spectral shapes are nearly identical.

KJCC will deliver the FITS file to the PI via an FTP server or a portable storage device.

- Once the correlation is complete, the FITS file will be prepared through post-processing. The KJCC will then notify the PI of the completion of the correlation processing via email. The email will include a temporary URL link through which the PI can access the FITS file.
- The PI should download the FITS file as soon as possible and verify it using their preferred analysis tool. Then, the PI should respond to the KJCC with either "Success" (indicating good data quality) or "Fail" (due to download failure, corrupted FITS file, poor data quality, etc.). In particular, if the response is "Fail", please include the error message when contacting the KJCC. A prompt response regarding the FITS file will help the KJCC resolve the issue as quickly as possible.
- The KJCC requests the PI to respond within two weeks of the email notification. If no response is received within four weeks, the KJCC will consider the PI's response as a "success".
- In the event of a "Fail", the KJCC will perform a URL check, file reconstruction, or re-correlation based on the type of failure. Following this, an updated

announcement will be sent to the PI via email.

  - In the case of "Success", correlation processing for that observation will be closed (at that time, the download link in the temporary URL will become unavailable), and the tapes or disk modules will be returned to the release pool for recycling.
  - The FITS file provided to the PI will be stored separately in the observation data archive. The PI is expected to analyze the data, conduct research, and publish the paper within a specified period, typically 18 months. After this embargo period, the FITS file in the archive will be made publicly accessible, allowing others to conduct research using the data in accordance with established procedures.

- **Archiving policy**
  The KJCC manages the archiving policy for observational data, CODA files, and FITS files as outlined below.

  - All VLBI data obtained with the KVN are accessible for collaborative purposes and will be used exclusively by the PI without external sharing for 18 months following the observation. After this exclusivity period, all data will be stored on KASI's dedicated servers and made publicly available through the Science Data Portal (http://data.kasi.re.kr, see Figure 23).
  - CODA: If correlated data is used for astrometry or geodesy, it is permanently stored on the CODA server. Otherwise, the correlated raw data and CODA file system are deleted after receiving a response from the PI.
  - FITS: it is permanently archived on the Archiving Server.

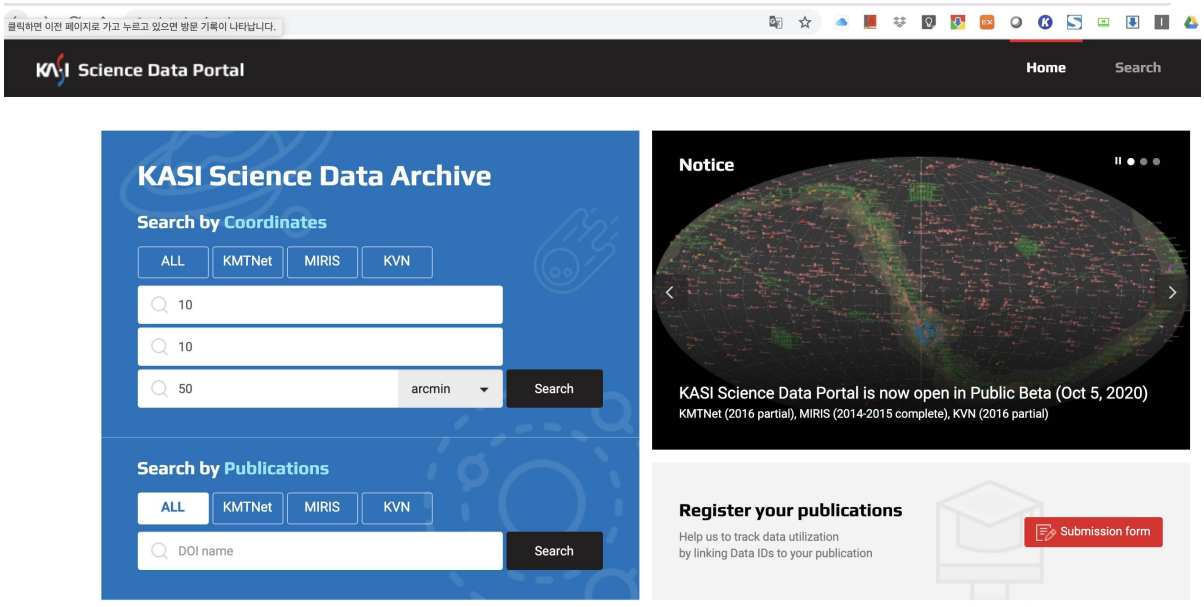

Figure 23: Initial screen of the KASI Science Data Portal

2.5 Calibration for VLBI observations

System temperatures in Kelvin ($T_{\rm sys}$) are measured during observations at KVN stations once every user-specified interval (default 10 sec) to calibrate amplitude variation in time due mainly to atmospheric fluctuation. The measured $T_{\rm sys}$ is a sum of three temperatures: the receiver temperature, the spillover temperature, and the contribution of the atmosphere as described in Petrov et al. (2012) [8]. These $T_{\rm sys}$ values can be converted to SEFD (System Equivalent Flux Density) by dividing by the KVN antenna gains in K/Jy. The elevation dependence of the antenna gains is also corrected based on the normalized gain curves with lease-squared-fitted second-order polynomials as mentioned in previous Section 2.2.2.

Additional amplitude correction for the atmospheric opacity above an antenna is performed by conducting a sky tipping curve analysis according to the method described in Mangum (2000). In practice, the system temperatures ($T^*_{\rm sys}$) corrected for the atmospheric opacity are estimated based on the sky tipping curve measurements once every user-specified interval (default before and after an experiment). Further corrections are made to the KVN observations taken with 2-bit (4-level) sampling, for the systematic effects of the non-optimal setting of the quantizer voltage thresholds.

The amplitude calibrations with the KVN are accurate to 15 % or better at 22 and 43 GHz. However, it is recommended to observe a few amplitude calibrators during the scheduled observation time, allowing for (a) the assessment of the relative gains of KVN antennas and gain differences between IF-bands at each station, and (b) the confirmation of the correlation coefficient correction assuming that you have contemporaneous source flux densities obtained with other VLBI networks independent of the KVN observations.

2.6 KVN geodetic VLBI measurement

Obtaining accurate antenna positions is important in the VLBI system, especially for high precision astrometry. KVN antenna positions are regularly monitored using GPS and geodetic VLBI observations. The K band geodesy VLBI program between KVN and VERA started in 2011. Current KVN antenna positions (see Figure 24) were obtained from the KaVA K band geodesy on January 24, 2014. The typical 1-sigma errors of geodetic solutions are about 0.4 cm in the X, Y, and Z directions. Based on 22-epoch KaVA K band geodetic observations from September 2012 to December 2016, uncertainties of KVN antenna positions are $\sim$ 2.38 cm at KYS, $\sim$ 2.55 cm at KUS, and $\sim$ 1.58 cm at KTN.

The accurate positions of the KVN antennas were recently derived from IVP measurements using GNSS. These are described in Section 2.1.3.

3 Observing proposal

3.1 Observing mode

3.1.1 Multi-frequency observation

Simultaneous multi-frequency observation is a unique capability of the KVN, with which we can calibrate out the short-term phase fluctuations at higher frequency data by referenc-

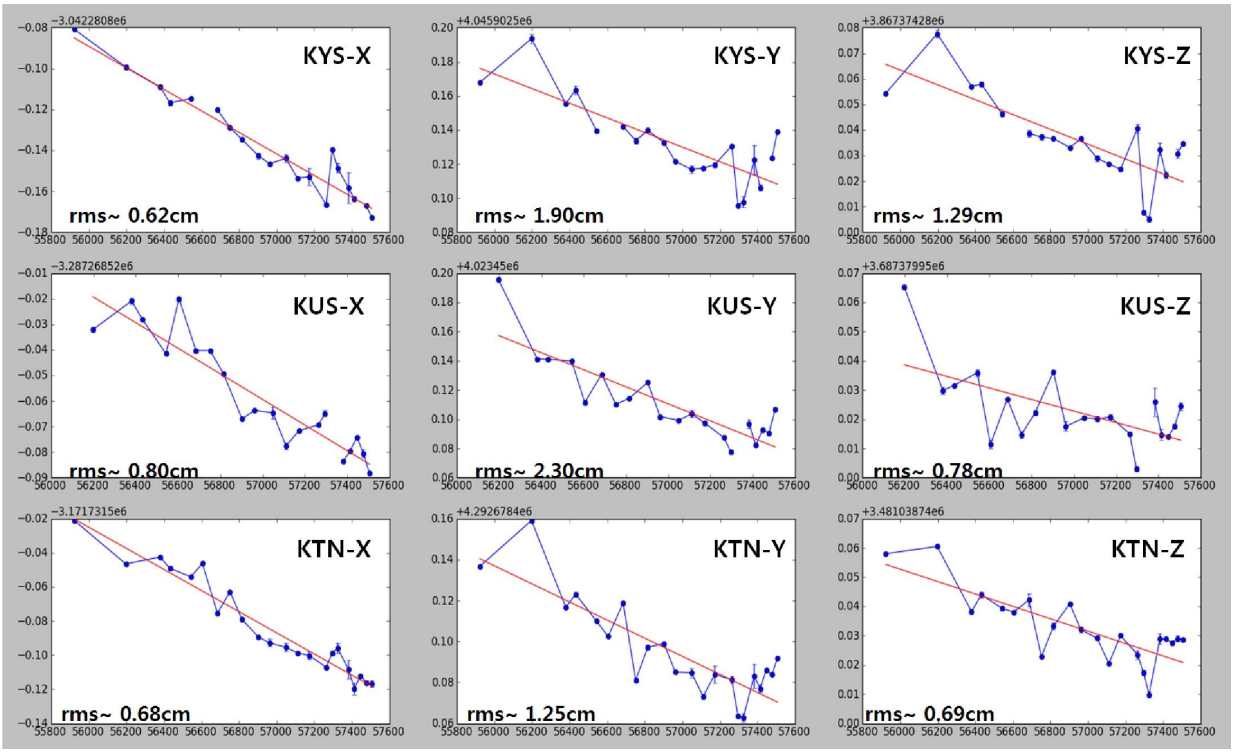

Figure 24: The trend of KVN antenna positions (IVP) in the ITRF 2014 coordinate system. The x and y axes are MJD and X, Y, and Z in meters. The linear fitting is applied to the measurements, shown as red line, and its deviation is also presented in each axis as "rms".

ing the phase solution obtained from lower frequency data. This phase referencing technique allows us to integrate the data for a time scale much longer than the coherent time scale of atmospheric phase fluctuation and so to observe weak sources at mm-wavelength efficiently. For multi-frequency observations, we can select up to 8 IF signals (= 4 bands × 2 polarizations). The observation technique for a simultaneous multi-frequency observation can be summarized by a formula as shown in Figure 25.

3.1.2 Fast position switching observation

The maximum mechanical slewing speed and acceleration of the KVN antenna are 3 °/sec and 3 °/sec^2, respectively; however, we use the reduced values of 2 °/sec and 2 °/sec^2. Due to these high speed and acceleration rates, the KVN antenna can quickly switch its pointing from the target to calibrator.

3.1.3 Recording rate

The signal output from an OCTAD is highly flexible, with a maximum rate of 32 Gbps. Starting from the 2026B season, each KVN station is equipped with two OCTAD backends, enabling the simultaneous observation of eight IF signals (4 bands × 2 polarizations). The previous backend, Fila10G, which supported 2 Gbps (1 × 512 MHz), 4 Gbps (2 × 512 MHz), and 8 Gbps (4 × 512 MHz), has now been replaced by the OCTAD.

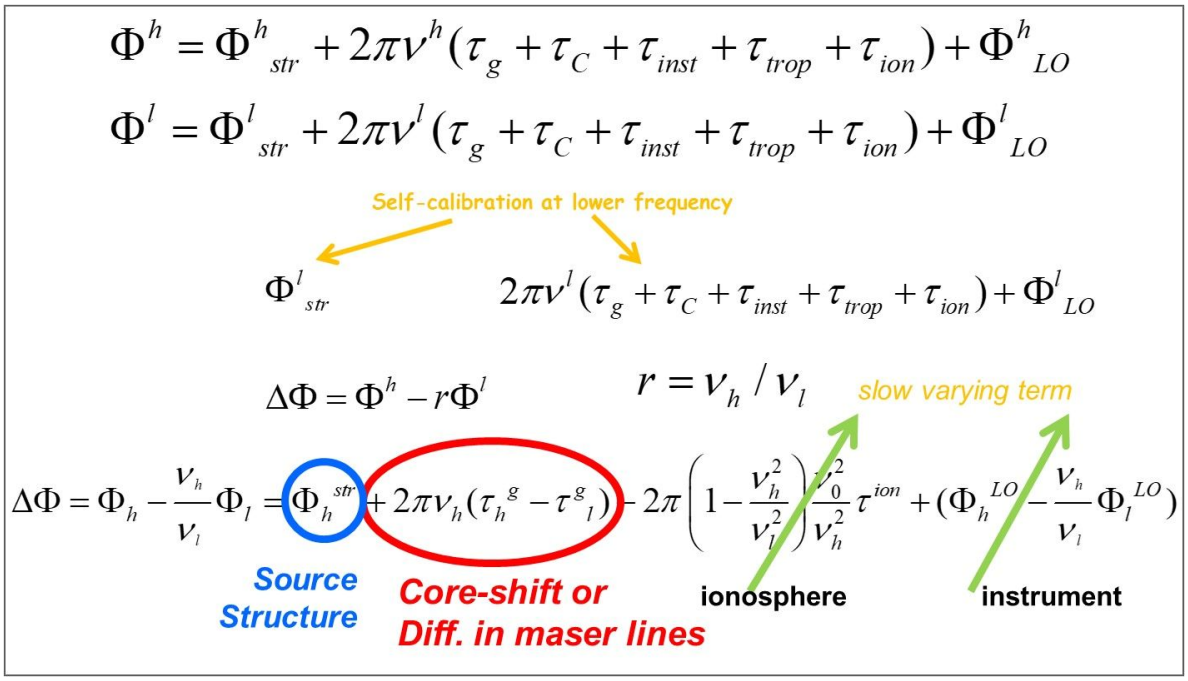

Figure 25: Scheme of Simultaneous Multi-frequency Calibration

3.2 Angular resolution

Table 13 shows the maximum lengths (B) of the KVN baselines in km and the corresponding resolutions ($\theta_{\rm HPBW}$) in milli-arcsecond (mas), which is estimated as $\theta_{\rm HPBW}$ (mas) $\sim 20627 \cdot \lambda$(mm)/B(km).

Table 13: Angular resolutions at each KVN baseline and frequency

Baseline	B (km)	$\theta_{\rm HPBW}$ (mas)			
		22 GHz	43 GHz	86 GHz	129 GHz
KYS–KUS	305.0	9.1	4.7	2.4	1.6
KUS–KTN	358.8	7.8	4.0	2.0	1.3
KTN–KYS	478.0	5.8	3.0	1.5	1.0
KPC–KYS	133.1	20.9	10.8	5.4	3.6
KUS–KPC	232.6	12.0	6.2	3.1	2.0
KTN–KPC	505.8	5.5	2.9	1.4	0.9

3.3 Baseline sensitivity

Table 14 shows sensitivities of the KVN baselines as follow: (1) frequency band, (2) nominal frequency range of KVN receivers, (3) system temperature, (4) typical KVN system-equivalent-flux-density at zenith, (5) antenna gain at the optimal elevation, (6) typical KVN baseline sensitivity for the aggregated recorded data rate of 1024 Mbps, the integration time

of 100 sec (K band), 60 sec (Q band), and 30 sec (W/D band), and the bandwidth of 256 MHz, and (7) typical KVN 3-baseline image sensitivity for the on-source integration time of 8 hr.

Table 14: Baseline sensitivity of the KVN

Freq. band	Freq. range (GHz)	$T_{\rm sys}$ (K)	SEFD (mJy)	Gain (K/Jy)	ΔS (mJy)	ΔI (mJy/beam)
(1)	(2)	(3)	(4)	(5)	(6)	(7)
K	21.25–23.25	100	1129	0.089	12	0.2
Q	43.11–44.11	150	1715	0.087	18	0.3
W	85–95	200	2073	0.072	29	0.6
D	125–142	250	3041	0.049	54	1.0

3.4 Support for International Multi-freq. VLBI Observations

The KVN telescopes are employed for active research observations in conjunction with the EAVN, EVN, and GMVA telescopes as part of an international collaborative observing network. Specifically, they serve as the primary axis of the EAVN. For more information on international joint observations, please refer to the EAVN Status Report. At present, the Yebes (Spain) and the Nobeyama (Japan) are equipped with receiving systems and backends for simultaneous K/Q/W band observations. The Italian telescopes–Notto, SRT, and Medicina–are in the process of upgrading their capabilities for W-band observations, utilizing CTR receivers developed and distributed by the KVN Center of the KASI. These telescopes are expected to be available for joint observations in 2027. According to the latest data, there are currently nine international telescopes (including the KVN & Sejong telescope) capable of conducting simultaneous K/Q band observations. Furthermore, six international telescopes (including the KVN telescopes) are capable of simultaneous K/Q/W band multi-frequency observations. Looking ahead, we expect a significant increase in joint observational opportunities during the 2027–2028 period, particularly with the integration of the three Italian telescopes, as well as the German Effelsberg and Finnish Metsähovi telescopes.

4 Observation and Data Reduction

4.1 Preparation of observation and correlation

4.1.1 General information

For the accepted proposals, the users have to prepare the observing schedule file before the observation. The observer who is not familiar with the KVN system is recommended to consult contact persons of the KVN group to prepare schedules, especially for some observations such as phase referencing, polarimetry, and/or spectral line, etc. Comprehensive

information regarding the observation planning and scheduling process is available on the KVN website[2].

4.1.2 Observation

All KVN experiments should be scheduled using the VEX (VLBI experiment) file. You can either edit and modify the KVN VEX example files or use the VLBA scheduling program SCHED[3]. It is recommended to use SCHED for your scheduling because SCHED provides useful information and many aspects of planning VLBI observations, and you can also avoid many mistakes arising from editing the VEX manually. The user needs to submit the VEX or key files two weeks before the observation. KVN AOC staff will check your schedule and proceed with the observations.

4.1.3 Correlation

Following the observation, the Daejeon correlator or DiFX correlator will perform the correlation procedure in accordance with the parameters that were provided. In order to release and recycle the disk modules and storage used for observation, the user is required to review the correlated data and report if the correlation was correctly performed. If there are any issues, re-correlation may be required. **The raw data disk modules used for the observations will, in principle, be discarded one week after the correlation process.** For further details, please refer to the correlation status report.

4.2 Data reduction

4.2.1 VLBI data reduction with AIPS

Here we introduce a very brief way of reducing VLBI data with KVN (or EAVN). For more detail, please have a look at the data reduction manual[4]. Figure 26 shows one of the procedures for reducing the KVN (or EAVN) observations.

5 Further information

Contact address It is possible for users to contact any staff member of the KVN by email (see Table 15). The official website[5] also provides various types of information.

[2] https://radio.kasi.re.kr/kvn/user_support.php
[3] http://www.aoc.nrao.edu/~cwalker/sched/sched.html
[4] https://radio.kasi.re.kr/eavn/user_support.php
[5] http://kvn.kasi.re.kr

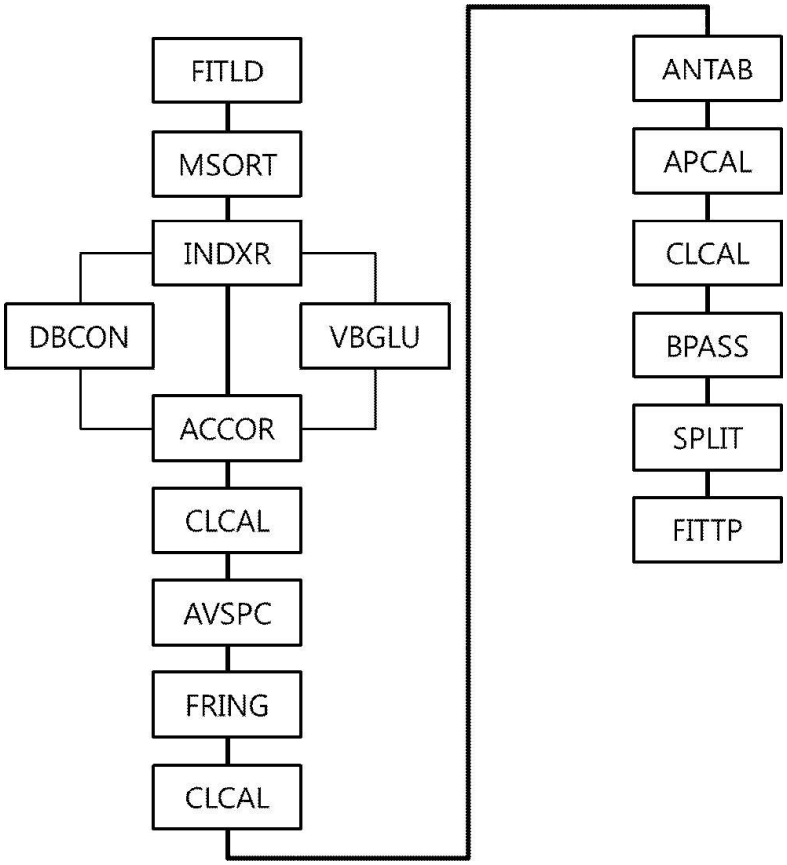

Figure 26: Data reduction flow chart with AIPS

Table 15: Contact information

E-mail	Subject
kvnprop@kasi.re.kr	Proposal submission and informing its result
kvnobs@kasi.re.kr	Observing schedule submission, observation-related requests and questions for the accepted proposal only
kjcc@kasi.re.kr	Correlated data distribution and correlation-related requests
kvnhelp@kasi.re.kr	General questions including scheduling, observations, systems, and so on (regardless of the proposal acceptance)

References

[1] S.-S. Lee, L. Petrov, D.-Y. Byun, J. Kim, T. Jung, M.-G. Song, C. S. Oh, D.-G. Roh, D.-H. Je, S.-O. Wi, B. W. Sohn, S.-J. Oh, K.-T. Kim, J.-H. Yeom, M.-H. Chung, J. Kang, S.-T. Han, J.-W. Lee, B. G. Kim, H. Chung, H.-G. Kim, H. Ryoung Kim, Y.-W. Kang, and S.-H. Cho, "Early Science with the Korean VLBI Network: Evaluation of System Performance," The Astronomical Journal, vol. 147, p. 77, Apr. 2014.

[2] I. de Pater, R. J. Sault, M. H. Wong, L. N. Fletcher, D. DeBoer, and B. Butler, "Jupiter's ammonia distribution derived from VLA maps at 3-37 GHz," Icarus, vol. 322, pp. 168–

191, Apr. 2019.

[3] M. Maris, E. Romelli, M. Tomasi, A. Gregorio, M. Sandri, S. Galeotta, D. Tavagnacco, M. Frailis, G. Maggio, and A. Zacchei, "Revised planet brightness temperatures using the Planck/LFI 2018 data release," Astronomy and Astrophysics, vol. 647, p. A104, Mar. 2021.

[4] S.-T. Han, J.-W. Lee, J. Kang, D.-H. Je, M.-H. Chung, S.-O. Wi, T. Sasao, and R. Wylde, "Millimeter-wave Receiver Optics for Korean VLBI Network," International Journal of Infrared and Millimeter Waves, vol. 29, pp. 69–78, Jan. 2008.

[5] S.-T. Han, J.-W. Lee, J. Kang, C.-S. Oh, D.-Y. Byun, D.-H. Je, M.-H. Chung, S.-O. Wi, M. Song, Y.-W. Kang, S.-S. Lee, S.-Y. Kim, T. Sasao, P. F. Goldsmith, and R. Wylde, "Korean VLBI Network Receiver Optics for Simultaneous Multifrequency Observation: Evaluation," Publications of the Astronomical Society of the Pacific, vol. 125, p. 539, May 2013.

[6] A. T. Deller, S. J. Tingay, M. Bailes, and C. West, "DiFX: A Software Correlator for Very Long Baseline Interferometry Using Multiprocessor Computing Environments," , vol. 119, pp. 318–336, Mar. 2007.

[7] A. T. Deller, W. F. Brisken, C. J. Phillips, J. Morgan, W. Alef, R. Cappallo, E. Middelberg, J. Romney, H. Rottmann, S. J. Tingay, and R. Wayth, "DiFX-2: A More Flexible, Efficient, Robust, and Powerful Software Correlator," , vol. 123, p. 275, Mar. 2011.

[8] L. Petrov, S.-S. Lee, J. Kim, T. Jung, J. Oh, B. W. Sohn, D.-Y. Byun, M.-H. Chung, D.-H. Je, S.-O. Wi, M.-G. Song, J. Kang, S.-T. Han, J.-W. Lee, B. G. Kim, H. Chung, and H.-G. Kim, "Early Science with the Korean VLBI Network: The QCAL-1 43 GHz Calibrator Survey," The Astronomical Journal, vol. 144, p. 150, Nov. 2012.